9-2006

Scaling Flight Tests of Unmanned Air Vehicles

Jeevani I. Abeygoonewardene

SCALING FLIGHT TESTS OF UNMANNED AIR VEHICLES

THESIS

Jeevani I. Abeygoonewardene, Captain, SLAF

AFIT-GAE-ENY-06-S01

DEPARTMENT OF THE AIR FORCE
AIR UNIVERSITY
AIR FORCE INSTITUTE OF TECHNOLOGY

Wright-Patterson Air Force Base, Ohio

AFIT-GAE-ENY-06-S01

SCALING FLIGHT TESTS OF UNMANNED AIR VEHCILES

THESIS

Presented to the Faculty

Department of Aeronautics and Astronautics

Graduate School of Engineering and Management

Air Force Institute of Technology

Air University

Air Education and Training Command

In Partial Fulfillment of the Requirements for the

Degree of Master of Science in Aeronautical Engineering

Jeevani I. Abeygoonewardene, BS

Captain, SLAF

September 2006

AFIT/GAE/ENY/06-S01

SCALING FLIGHT TESTS OF UNMANNED AIR VEHICLES

Jeevani I. Abeygoonewardene, BS
Captain, SLAF

Approved:

/signed/

David R. Jacques (Chairman) date

/signed/

Paul A. Blue (Member) date

/signed/

Mark F. Reeder (Member) date

Abstract

Increasing technological advances and research interest in unmanned air vehicles (UAVs), have led to the need for having safe, inexpensive and effective means of experimenting with their fight performance and surveillance capabilities. Work has previously been done in areas of controlling, analyzing, and predicting cooperative and autonomous operations of UAVs and other vehicles. In addition, there are well established guidelines for scaling experiments in fluid mechanics, where geometric, kinematic and dynamic similarity is obtained by formulating problems in terms of non dimensional variables using dimensional analysis. However, little or no work has been done in developing experiments or guidelines for air vehicles and their sensors. The currently available experiments for such purposes, which are designed around commercially available equipment, have not been standardized and cannot be related to the real systems and the real requirements.

The analysis done in this research provides an important step in setting up guidelines for experimental scaling of flight tests of UAVs. This makes it possible to use computer simulations and ground hardware experiments in a useful way for performance evaluations before having to fly the actual vehicle. Equations and simulations used have been defined in non-dimensional terms in order to allow for a scale independent approach as per the Buckingham Pi theorem. Comparisons have been drawn of flight and sensor performance characteristics between a nominal wide search area vehicle and two surrogate hardware systems having widely varying operating characteristics.

Acknowledgements

I would like to express my sincere appreciation to my thesis advisor, Dr. David Jacques and the rest of my thesis reading committee (Maj. Paul Blue and Dr. Mark Reader). A special thanks to Dr. Jacques for providing such good advice and guidance, spending endless hours to discuss important issues on my research, and point me in the right direction. Thanks to Maj. Blue who was always there with patience to help me not only with my thesis, but throughout my tenure at AFIT.

I would like extend my thanks to Mrs. Annette Robb, for being such a wonderful IMSO, and my “American Mom”. Thanks to my wonderful sponsor and dear friend Capt. Theresa Beaver for lending a helping hand throughout my stay. I would not have overcome the “cultural shock” without you. I am grateful to Ms Lynn Curtis for all the times she helped to squeeze me into Dr. Jacques’s busy schedule. Thanks to my friends Jennifer Andrews, Michael Hines, John Scarlette, Anna Gunn-Golkin, Michelle Gigante, Felicia Harlow and Tiffany Donahue for all their support, and for making my stay in the US a memorable one.

My family also deserves a fair share of credit for this endeavor. Thanks to my parents for their continued encouragement, inspiration and support throughout the years.

To my husband: thanks for your love, understanding and support, especially when we had to spend the first two years of our wedded life apart so that I could continue my education at AFIT. Thanks for always being there for me just a phone call away with your kindness and enduring patience, especially when times got rough for me on the other side of the world.

Finally, I would like to thank God, through whom all things are possible, for all His blessings, and giving me the strength to complete this research to the best of my ability.

Jeevani I. Abeygoonewardene

Table of Contents

Page

Page

List of Figures

Figure Page

List of Tables

List of Symbols

α	$\equiv$	Slant Angle
A	$\equiv$	Area
A_s	$\equiv$	Area of Battle Damage
ΔA	$\equiv$	Area of the Sensor Footprint
c	$\equiv$	ROC Parameter
d	$\equiv$	Down Range
D	$\equiv$	Total Distance Traveled
F_L	$\equiv$	Frame Length
F_S	$\equiv$	Frame Separation
γ	$\equiv$	Depression Angle
g	$\equiv$	Minimum g Limit
G	$\equiv$	Gravitational force of the Earth
h	$\equiv$	Altitude
λ	$\equiv$	Poisson Probability Law Parameter
λ_{A_T}	$\equiv$	Poisson Probability Law Parameter of a True Target Attack
$\lambda_{A_{FT}}$	$\equiv$	Poisson Probability Law Parameter of a False Target Attack
λ_T	$\equiv$	Poisson Probability Law Parameter of a True Target

λ_{FT} ≡ Poisson Probability Law Parameter of a False Target

l ≡ Distance the Aircraft moves away from its Flight Path during Turn

l_t ≡ Characteristic Target Length

μ ≡ Target Density Parameter

$\mu_{A_{FT}}$ ≡ Density of False Target Attacks in A_S

μ_{A_T} ≡ Density of True Target Attacks in A_S

μ_{FT} ≡ Density of False Targets in A_S

μ_T ≡ Density of True Targets in A_S

NT ≡ Number of True Targets

NFT ≡ Number of False Targets

O_L ≡ Frame Overlap

Π ≡ Pi group

P ≡ Total Pixels per Frame

P_A ≡ Probability of Attack

P_E ≡ Probability of Encounter given a target in search area

P_K ≡ Probability of Target Kill

P_{TR} ≡ Probability of True Target Report

P_{FTR} ≡ Probability of False Target Report

P_t ≡ Pixels on Target

ρ_T ≡ Pixels Density

r ≡ Turn Radius

s ≡ Slant Range

Θ ≡ Swath Angle

τ ≡ Time of a False Target Attack

t ≡ Time of a True Target Attack

T ≡ Time Duration of Mission

V ≡ Vehicle Velocity

w ≡ Frame Width

x ≡ Normalized Space or Time

X_S ≡ X Scale

Y_S ≡ Y Scale

z ≡ Frame Length

List of Abbreviations

Abbreviation		Page
ATR	Autonomous Target Recognition	28
F	False	71
N	No	71
NTA	Number of Target Attacks	68
NFTA	Number of False Target Attacks	68
NTK	Number of Target Kills	74
ROC	Receiver Operating Characteristic	25
T	True	71
UAV	Unmanned Air Vehicle	04
VFOV	Vertical Field of View	30
Y	Yes	71

SCALING FLIGHT TESTS OF UNMANNED AIR VEHCILES

I. Introduction

Motivation

Currently in the vehicle dynamics and control community it is common practice to use full scale models to physically verify performance and validate simulated results of various experiments. This method, when successful results are delivered for the given experiment, can prove to be reliable and economic since the test carried out on the actual vehicle could carry a high risk factor of safety and cost. There are several reasons why a control engineer would prefer to experiment with scaled systems. Two key factors are cost and safety because scaled systems are often less expensive and less hazardous to work with than full scale systems. Integration, modularity, scalability and transparency are other motivational factors. These are more obvious, especially when it comes to flight vehicles. This research is focused on designing scaled test beds that will minimize the gap between simulation studies and full-sized hardware experiments.

From a historical perspective, the concept of scaling goes back to 1638, when Galileo first introduced “scaling” and “physics” in his treatise *Disclosures and Mathematical demonstrations Concerning Two new Sciences pertaining to Mechanics and Local Motions* [1]. The very famous Froude number was named after a ship construction engineer who developed a methodology to evaluate ship designs. Froude modeled important relationships with regard to ship dynamics, such as the relationship between wave production and energy losses. He accomplished this by using scaled ships to carryout simulations, thereby eliminating catastrophic design failures that were inherent in the construction of ships. The Wright Brothers’ success in developing the first heavier than air aircraft was due in part to their extensive experiments of flight dynamics carried out in their wind tunnel [2]. In the 1960s the lunar rover designs were experimentally tested through the use of scaled vehicles driven on rough surfaces. The experimental results obtained from the tests were later used to design the Mars Sojourner robot [3].

The Illinois Roadway Simulator (IRS) is an experimental test bed that consists of scaled vehicles that run on a simulated road surface. Similar to a wind tunnel, where an experimental scaled flight vehicle is held fixed in an incoming flow of air, IRS holds the vehicles fixed relative to an incoming road surface [4].

The advantages of using scaled test beds are that they prove to be much cheaper than the full scaled experiment and are typically much less hazardous. In addition, they enable the tester to simulate a variety of operating conditions that would be difficult to create in a real world scenario. For example, when simulating an aircraft's environment, it is possible to create an atmosphere such that the vehicle dynamics could be tested at the edge of the flight envelope and beyond. This would be nearly impossible and tremendously dangerous if tested with a full sized model in the real world environment.

Previous work

Mobile Robots. The control of mobile robots, single and multiple, both from centralized and decentralized controllers, is a problem that has been subject to a wide range of research activity in both the engineering and artificial intelligence field. In the recent past there has been increased interest on the systems composed of multiple autonomous mobile robots exhibiting cooperative behavior. Groups of robots are constructed by many researchers with the aim of studying issues such as group architecture, resource conflict, origin of cooperation, learning and geometric problems. Coordination and interactions of multiple intelligent agents have been actively studied in the field of distributed artificial intelligence (DAI) since the early 1970s [5]. However the DAI field concerned itself mainly with problems involving software agents. In the 1980s, the robotics research community became very active in developing cooperative robots, beginning with projects that involved physical implementations and simulations of robot cooperative behavior.

During the experiments conducted in the Mobile Robot Laboratory at the Georgia Institute of Technology, supported by DARPA [6], formation performance on mobile robots was demonstrated, where the behavior was modeled on how each robot would move based on the behavior of other robots in the environment.

Although several experiments have been carried out with single and multi robot systems, none of these systems relate any of the test results to applications in disciplines other than the specific case. Experiments have been developed to model robots that carry out commands and behave in a cooperative manner; however, they show no potential of establishing a connection to flight testing of UAVs where similar concepts are applied in different scenarios by significantly different agent vehicles.

Unmanned Air Vehicles. Unmanned Air Vehicles (UAVs) are playing an increasingly prominent role in the defense and strategy programs of nations around the world. The ability to utilize UAVs in a variety of situations with minimum risk to human life makes them very attractive. Dramatic technological advances, especially in control systems, sensors and batteries have led to the development of highly versatile and efficient UAVs such as the Global Hawk, Predator, and also smaller, increasingly capable UAVs. These small UAVs and micro UAVs (MAVs) have a multitude of military applications; they can carry out reconnaissance, surveillance, battle damage assessment, and act as communication relays.

While military applications are not yet achieving their fullest potential, UAVs have a broad scope of application in the commercial field as well. Environmental monitoring, home land security, aerial surveillance and mapping, traffic monitoring, precision agriculture, disaster relief, and rural search and rescue are just a few of the areas that UAVs can be utilized apart from military applications. For many of these applications, increased reliability, extended capability, user friendliness and profitability are essential.

Limited experimental research has been carried out regarding cooperative Control of UAVs. Experiments have been executed to address cooperative surveillance problems where a team of UAVs is directed to fly over a target with a specified time interval between the time over target for each vehicle [7]; however, results from experiments are not applicable to a universal case since they have a scope that is limited to specific mission and vehicle capabilities due to physical and technological constraints.

The increased interest in UAVs has triggered research activity in the area of cooperative control and wide area search capabilities. As intriguing as it may seem, research and experimentation in this field has been restricted due to practical challenges of physically deploying multiple airborne agents and cost factors. In this light it is seen that the ability to perform flight tests of UAVs on some other platform, which can model the various subsystems such as sensors, and guidance and control systems would be of immense use.

Presently, there are several platforms that model certain subsystems of UAVs. The Variable Stability Test Aircraft (VISTA) [8], owned by the United States Air Force, is one such test aircraft that provides flight tests, evaluation, and in-flight simulation capabilities for guidance, navigation and control systems and cockpit display research and development. While the VISTA offers a UAV test bed platform that is capable of simulating actual flight hardware, software, and flight dynamics relatively risk free in the actual mission environment, it has the limitation of being able to test only those aircraft whose performance characteristics fall within its flight envelope. Furthermore, it is extremely expensive to operate.

Wind Tunnels. The primary goal of many wind tunnels is conducting experiments using scale models, so that the behavior of full scale vehicles can be predicted based on the results obtained. In order to obtain similarity of flow governed by basic aerodynamic equations sets of non-dimensional equations have been developed [9]. Geometry, fluid speeds, pressure, density, temperature and time have been nondimensionalized as ratios to some reference. For example, residence time is nondimensionlized as a ratio to the time for a fluid particle to travel a reference length at the speed of the flow far away from the body of the experimental specimen. Similarity parameters such as Froude number, Reynolds's number, and Mach number appear in nondimensional forms of fluid dynamic equations. If a model experiment has similar parameters to the full-scale application, then the model and the full scale flows will be dynamically similar; the nondimensional functions for fluid velocity components, density, viscosity, temperature and pressure coefficients, force and moment coefficients will be the same for the model and full scale vehicle. Thus, it is possible to obtain direct correlations between the results obtained from the scale model to actual vehicle flight or other data. Even though it is very difficult to match these similarity parameters in most wind tunnel experiments, the wind tunnel remains one of the most widely used, useful tools in the field of aerodynamics.

Other Scaled Vehicles and Test Beds. Many studies have been carried out with scaled vehicles, where they have been used as prototypes and test beds to test actual systems. In an experiment carried out at the Auburn University to investigate the influence of various properties on rollover propensity, a 1:10 scale remote controlled car was used (Figure 1). This car was controlled by a computer, and was modified to adjust center of gravity height and location, spring stiffness and roll center height. The model was validated by comparing the data from a 2001 Chevy blazer 4×2. Validation was achieved by the correlation between experimental results obtained by this scaled model and simulated dynamics [10].

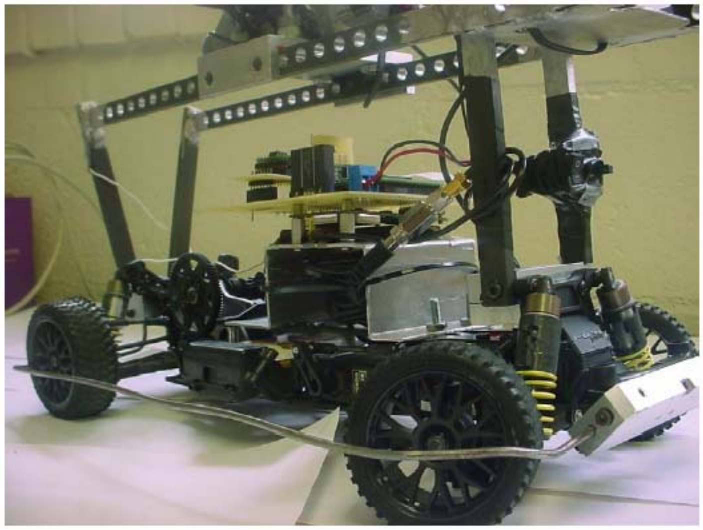

Figure 1. Scaled Vehicle used to test Roll over propensity of automobiles.

In other research carried out at the University of Delft, Netherlands, the project DAVINCI was developed for demonstration and validation of a scaled-model research facility that evaluates technologies and techniques for advanced vehicle control systems [11]. It employs scaled model cars with onboard sensors as experimental platforms to demonstrate longitudinal and lateral vehicle control, providing a good replication of the real system with less cost and effort. One such scale model, known as the “Davicar”, is shown in Figure 2. In the development of this project, the researchers used the Buckingham Pi theorem and dynamic similitude analysis to scale down this test vehicle so that it would closely approximate the real system; however, it was problem specific and could not be applied to a wide range of vehicles, operating environments and conditions.

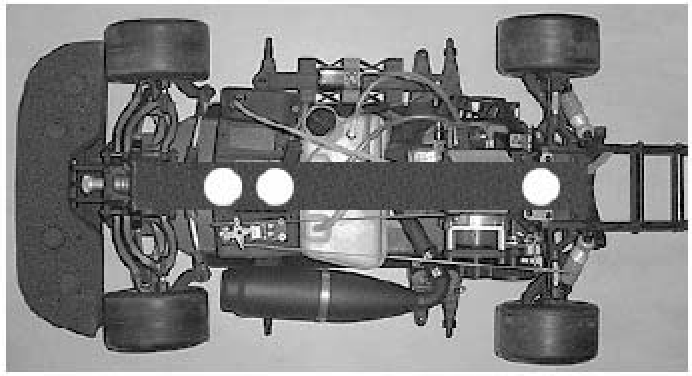

Figure 2. “Davicar”- Experimental testing scaled vehicle

In the field of automotive research, scaled vehicles and vehicle components have been used extensively to determine the performance and dynamics of actual full-sized vehicles. In an experiment carried out to perform a non-dimensional analysis of vehicle tires, scaled vehicle tires were used to investigate the forces generated by actual vehicle tires [12]. The behavior of actual tires was defined by the use of various formulas based on the characteristics of the tires. Scaled tires were later run on a treadmill set up to test the static response to various speed, slip, and normal force conditions. In this research, the goal was to prove that the behavior of tires was independent of size. Here again, even though the researchers successfully scaled the experiment to achieve desired results the methodology was problem specific.

Methodology-Buckingham Pi Theorem

Introduced by E. Buckingham in 1914, The Buckingham Pi theorem is a key theorem in dimensional analysis. It states that for a given physically meaningful equation involving *n* physical variables, expressed in terms of *k* independent fundamental physical quantities, then the original expression is equivalent to an equation involving a set of $p = n - k$ dimensionless variables constructed from the original variables. It provides a means of computing sets of dimensionless parameters from the given variables, even if the form of the equation is still unknown. The choice of dimensionless parameters is not unique, it simply provides a way of generating sets of dimensionless parameters, where the most 'physically meaningful' parameters will not always be chosen. Two systems for which these parameters coincide are called *similar*; they are equivalent for the purpose of the equation, and the experimentalist who wants to determine the form of the equation can choose the most convenient one.

In order for a scaled model to be comparable and compatible in modeling full-sized vehicles, they need to have dynamic similarity. This is achieved when the pi groups (dimensionless group) of the two vehicles match. Dynamic similarity is shown by using this theorem to replace the dimensional physical parameters with dimensionless products and ratios. Very often it is seen that once the scaled model is developed the actual vehicle is modified to match its pi groups, or the pi groups of a scaled model have similarity only to a certain subset of UAVs. The concern here is to achieve the reverse of the former; develop a scaled vehicle that can meet the full range of dynamic similarities for a general UAV or autonomous munition platform.

Research Statement

The focus of this research will be on developing scaling techniques for UAV flight test experiments such that the results of multi-vehicle experiments (using ground or air vehicles) can be used to predict the performance of actual UAV system concepts.

Comparisons to various vehicles will be drawn relative to a nominal autonomous air vehicle. For the purpose of this research, two types of surrogate vehicles will be taken into consideration: one having a slower velocity and one a higher velocity than the nominal case. Primary calculations will be performed using the Buckingham Pi theorem to enable a dimensional analysis.

Behavior of various vehicles was simulated in terms of basic flight dynamics and sensor characteristics (i.e. search, detection, declaration, and attack). A computer simulation was developed and run for two primary cases:

- The fixed velocity and turn rate option
- The fixed target size and turn rate option

These results will be analyzed in order to ascertain if in fact it is possible to scale the different vehicles and the operating characteristics of their sensors, in order to provide test expedient surrogates for a targeted air vehicle concept of interest.

Assumptions

Three types of vehicles were considered for the purpose of this research: a nominal wide area search vehicle and two surrogates with contrasting performance characteristics. It should be noted that the nominal case used for each experiment could differ according to the data and facilities available. It was assumed that the air vehicles were flown in un-accelerated level flight with no external disturbances acting on them, while it was assumed that the ground vehicles traveled on a flat, no-slip surface. Relationships between vehicle dynamics and Receiver Operating Characteristics (ROC) of the sensors were determined through intuition since no predefined relationships were available. Data obtained for the purpose of analysis originated from computer simulations and not actual hardware experiments. Statistical methods were used for the distribution of agents and target attack and recognition algorithms. A Poisson probability distribution of targets approximated by a uniform distribution was used for true and false target dispersion.

Outline of the Document

Chapter II defines the various vehicle dynamics and sensor characteristics that were taken into consideration. It sets up the design variables and defines the model in terms of the associated probability parameters for the problem set up and computer simulation problem.

Chapter III introduces and describes the Buckingham Pi theorem and its application, which is the basic methodology of this research. Pi groups are developed with the aid of the design variables identified in Chapter II. The significance and relevance of the pi groups in drawing dynamic similitude between various vehicles are then discussed.

Chapter IV describes the computer simulation that was developed in order to show the effects of scaling on vehicle operation, and sensor performance. This chapter analyzes the results obtained from the simulation and compares the attack values to the expected values derived from analytical probability expressions. The simulation is run for different cases (vehicles) and the results are compared.

Chapter V is a discussion of the contributions the research provided. The work is concluded with recommendations for future interest on the subject.

II. Problem Setup and Definitions

A first step will be to identify the basic variables and parameters of a wide area search flight vehicle, such that independent sets of equations can be developed to tie together how each variable and parameter effect each other and the performance of the aircraft. From the available parameters, pi groups are developed such that they could be compared with those of the actual vehicle, when later applying the Buckingham Pi theorem.

The wide area search vehicle is an autonomous UAV that searches the ground using a sensor employing Autonomous Target Recognition (ATR). The sensor footprint will be assumed to be rectangular, and any sort of distortion due to geometry and motion is ignored for the purpose of this initial investigation. The attention of the research is limited to a wide area search vehicle in un-accelerated and level flight that searches, identifies and attacks potential targets.

In this chapter, an analytical approach will be emphasized in order to capture the effectiveness of a wide area search vehicle. Applied probability theory is used to formulate and solve for probability of success in search and engagement.

Azimuthal Footprint

Consider a wide area search vehicle flying on a horizontal path at a constant velocity V and altitude h that is mounted with a sensor that generates a footprint that has a width w and a length z. The velocity to achieve any given search rate decreases as the minimum down range distance d is increased, with the swath angle θ held constant. The area search rate is a direct function of the vehicle velocity and width of the sensor foot print.

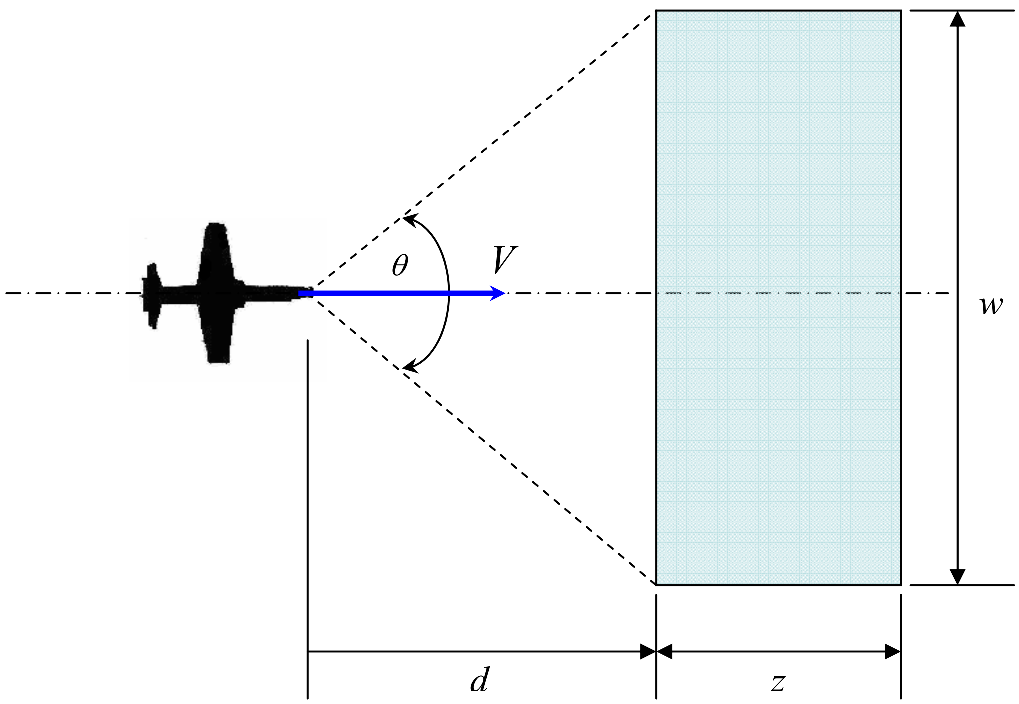

Figure 3. Azimuthal View of the Aircraft in Flight

From Figure (3) it can be seen that the swath angle of view of the sensor,

$$\theta = \tan^{-1}\frac{w}{d} \tag{1}$$

Area search rate,

$$\frac{dA}{dt} = w \cdot V \tag{2}$$

Vertical Footprint

Figure (4) illustrates the elevation view of an aircraft in straight and level flight at an altitude h. Many UAV sensors are designed to operate within a narrow range of depression angles, which will be assumed fixed for a given vehicle; thereby, the slant angle α would be a constant. For such a vehicle the only possibility of looking further away or changing its footprint size would be to gain or lose altitude.

The Vertical Field of View (VFOV) determines the frame length of the footprint and maximum slant range s. Maximum slant range and resolution determine pixels on target. Hence, it plays an important role in target recognition.

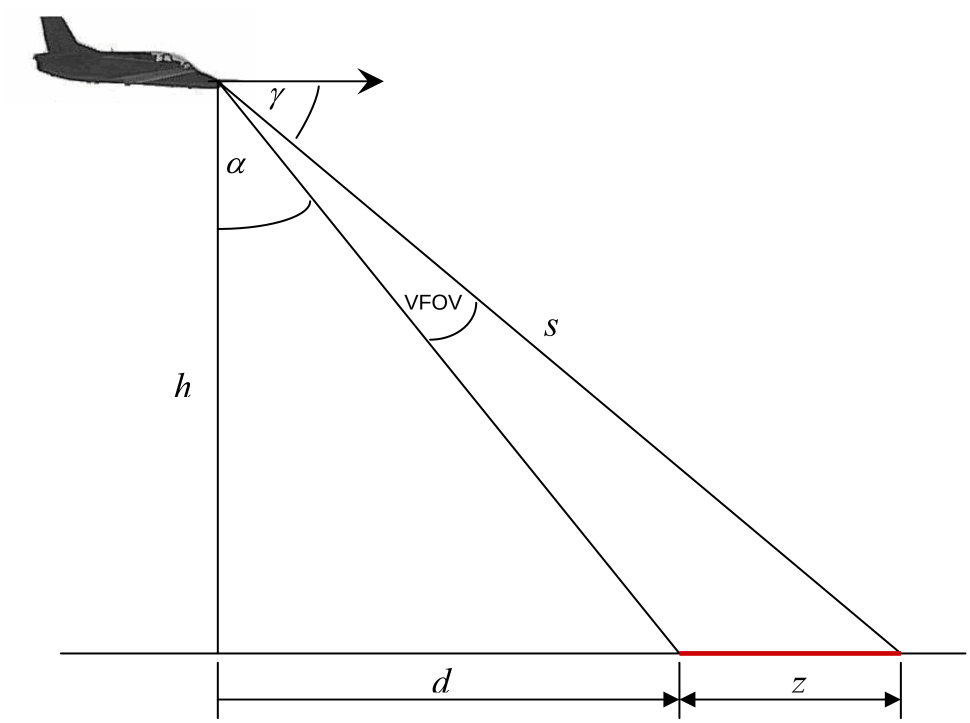

Figure 4. Elevation View of the Aircraft in Flight

Assuming level flight, the frame length z, the depression angle γ, and the slant range s can be calculated from Figure (4) for a given VFOV and h by,

$$z = h\tan(\tan^{-1}\frac{d}{h} + VFOV) - d \tag{3}$$

$$\gamma = \tan^{-1}\left(\frac{h}{d+z}\right) \tag{4}$$

$$s = h\cos(VFOV + \tan^{-1}\frac{d}{h}) \tag{5}$$

Selection of *VFOV* also determines the pixel density, since it determines frame size. The number of pixels available is an important characteristic of the sensor. The more pixels it is capable of placing on a target, the better the resolution will be, and the better and more accurate the identification will be. Pixel density ρ_T is specified in terms of total pixels per frame P and the area of the frame, and is given by,

$$\rho_T = \frac{P}{w \cdot z} \tag{6}$$

Aircraft Turn and Target Strike

Now consider the aircraft turning to detect or engage a target at the far edge of the search swath, at the nearest down range. The ability of the vehicle to reach this point during a first pass near the target is dependent on its minimum turn radius. The selection of down range should be such that the vehicle/weapon will be able to reach the target within its maximum maneuver capability after detecting and processing the target information. This will ensure a successful attack. Figure (5) illustrates the aircraft performing a maneuver to execute an attack on a target in its search swath.

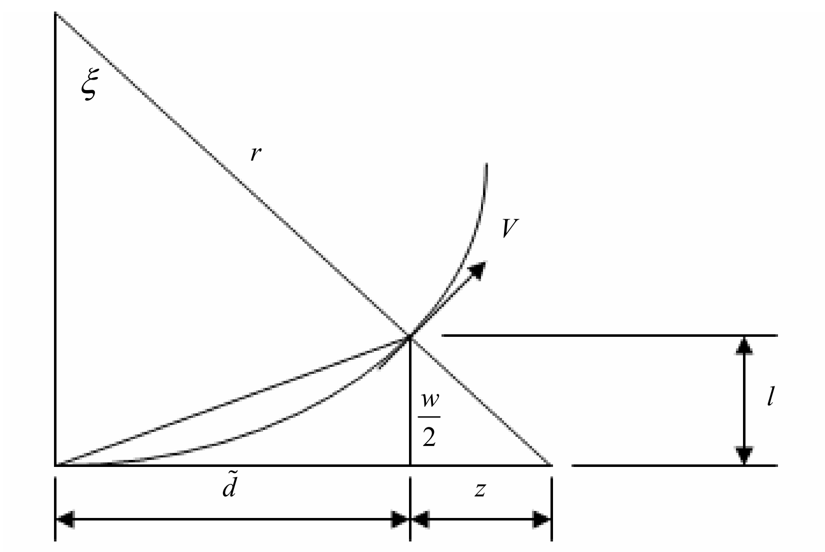

Figure 5. Aircraft Turning towards a Target

The term *l* represents the horizontal displacement of the aircraft when turns at an angle ξ with a turn radius *r*. The load *g*, which is the force due to acceleration, on the vehicle due to a turn of constant radius *r* is given by,

$$g = \frac{V^2}{r \cdot G} \tag{7}$$

where *G* is the acceleration due to the earth's gravitational force. Hence, if a vehicle's *g*-limit, which its maximum sustainable load, is denoted by g_{max}, then its minimum turn radius r_{min} is given by,

$$r_{\min} = \frac{V^2}{g_{\max} \cdot G} \tag{8}$$

From Figure (5) it can be seen that

$$\tilde{d} = rsin\xi$$

$$l = r - rcos\xi$$

When $$\tilde{d} = d$$

let $$\xi = \xi_d$$

where $\xi_d =$ (the turn angle resulting in a minimum turn radius turn until $\tilde{d} = d$).

Then,

$$d = rsin\xi_d \tag{9}$$

and

$$l = r - rcos\xi_d \,. \tag{10}$$

When the aircraft is turning under its maximum g limit (with a minimum turn radius), for it to be capable of a first pass engagement of any targets appearing in the search footprint, it is required that,

$$l_{\max} \geq \frac{w}{2} \qquad \text{when} \qquad \tilde{d} = d$$

where

$$l_{\max} = r_{\min} - r_{\min}\cos\xi_d = r_{\min}(1 - \cos\xi_d)\,.$$

Frame Overlap

Frame overlap ensures that any given target is wholly contained in at least one frame, so that frame processing can be independent (a necessity for processing delay time from pixels on target to target report and start of attack maneuver, if any, is to be held a minimum). The amount of frame overlap must be greater than the maximum target dimension to ensure a target will be contained entirely within a single frame. Frame length must exceed frame separation by the desired frame overlap. This places a requirement on frame formation time: the time available for frame formation is the frame separation divided by the vehicle search velocity, with allowance for scan retrace time. Figure (6) illustrates a search scenario yielding frame overlap. Frame overlap (O_L) is given by frame length F_L and frame separation F_S as shown below:

$$O_L = F_L - F_S \tag{11}$$

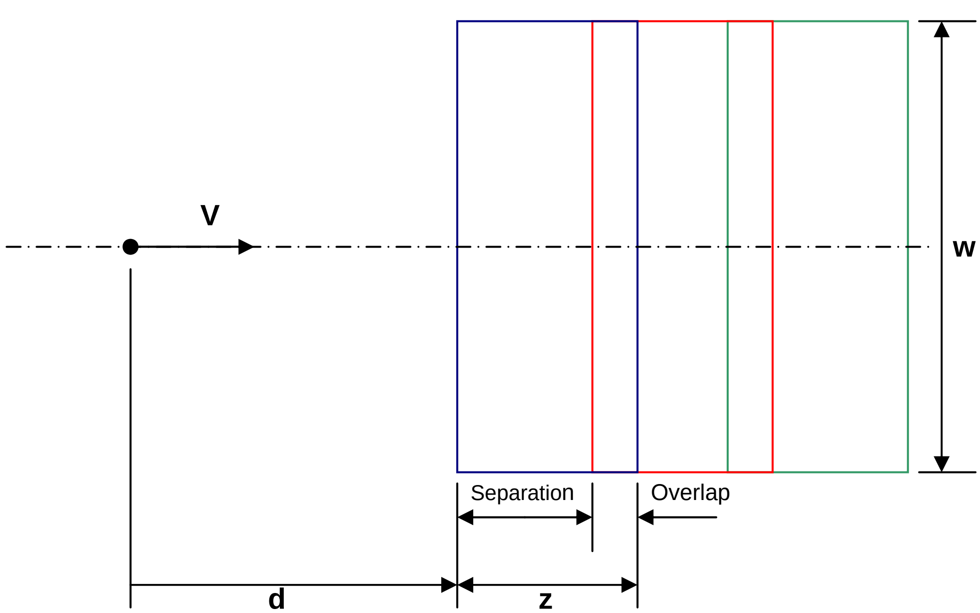

Figure 6. Straight Search Scenario yielding Frame Overlap

Poisson Field of Targets

A Poisson distribution will be assumed for the number of the true targets and false targets, the locations of which are approximated by a uniform distribution. Other distributions have been analyzed [13], but this research will limit itself to Poisson distributions. It expresses the probability of a number of events occurring in a fixed period of time if these events occur with a known average rate, and are independent of the time since the last event. A random variable whose sample space $S = \{0,1,2,...\}$ has the probability mass function $p(\cdot)$ with the parameter $\lambda > 0$ given by

$$p(f) = e^{-\lambda} \frac{\lambda^f}{f!} \quad , \quad f = 0,1,2,...$$

is said to obey the Poisson probability law with the parameter λ. It gives the probability that there will be exactly f occurrences.

The Poisson field of targets is characterized by the expected distribution of target densities (μ) such that when an area A is searched, the Poisson probability law parameter is

$$\lambda = \mu A \tag{12}$$

The Poisson parameter here represents the expected number of target encounters in area A.

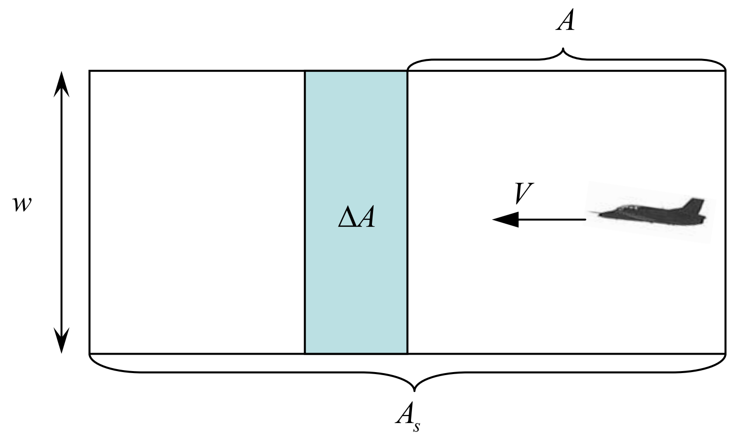

Figure 7. Rectangular Battle Space Area Definitions

Figure (7) depicts a rectangular battle space of area A_s being searched with an aircraft sensor generating a footprint that has area ΔA. A region of area A already searched, containing an expected number of true targets (*NT*) and an expected number of false targets (*NFT*), as is approximated in the simulation of this research, then the probability of any target being in A is

$$P\{\text{Any One True Target in } A\} = NT\,\frac{A}{A_s}$$

for a true target and

$$P\{\text{Any One False Target in } A\} = NFT\,\frac{A}{A_s}$$

for a false target.

The area searched can be denoted as

$$A = A_S \cdot x \tag{13}$$

where x is the fraction of the battle space area being searched. It can also represent a normalized area.

In addition, define,

$$\lambda_T = \mu_T A_S \tag{14}$$

$$\lambda_{FT} = \mu_{FT} A_S \tag{15}$$

where μ_T and μ_{FT} are respectively the expected densities of true and false targets in the battle space. Then the Poisson parameter for false targets is given by, $\lambda = \lambda_{FT} x$ and for true targets is $\tilde{\lambda} = \lambda_T x$. Target attacks have a Poisson parameter $\lambda_{A_T} x$ for true target attacks and $\lambda_{A_{FT}} x$ for false target attacks.

Define

$$\lambda_{A_{FT}} \equiv \mu_{A_{FT}} A_S,$$

where $\mu_{A_{FT}} = \mu_{FT}(1 - P_{FTR})$ represents the density of false targets in the battle space. The term P_{FTR} is the conditional probability that given a false target encounter, the Sensor/ATR correctly reports it to be a false target. Then the expected number of false target attacks in A is,

$$\mu_{A_{FT}} A = \lambda_{A_{FT}} x \tag{16}$$

Similarly for true targets,

$$\mu_{A_T} A = \lambda_{A_T} x. \tag{17}$$

These can be identified as the Poisson parameters for true and false target attacks. It is possible to convert a Poisson field of false targets or true targets to a Poisson field of false target attacks (FTAs) or true target attacks (TAs) as follows [14]:

$$\lambda_{A_{FT}} = (1 - P_{FTR})\lambda_{FT} \tag{18}$$

$$\lambda_{A_T} = P_{TR}\lambda_T \tag{19}$$

The term P_{TR} is the conditional probability that the sensor correctly recognizes a target, that is, it encounters a true target and reports it to be a true target as well. The sensor on the wide area search vehicle is assumed to have an Autonomous Target Recognition (ATR) system which makes target declarations based on stored target templates. Declarations are uncertain and both false target and missed target declarations are possible. Sensor performance is often characterized by how often the sensor makes its decision correctly. The confusion matrix represents the probability of both correct and incorrect target reports. The basic single objective confusion matrix appears as follows:

Table 1. Simple Binary Confusion Matrix

Object Encountered / Object Reported	True	False
True	P_{TR}	1- P_{FTR}
False	1- P_{TR}	P_{FTR}

The term $(1-P_{TR})$ represents the probability that when a target is encountered, the sensor mistakes it to be a false target and incorrectly reports it to be a false. The term $(1-P_{FTR})$ is the probability that the sensor encounters a false target and incorrectly reports it to be a true target. For this binary confusion matrix, the true positive fraction is P_{TR} and the false positive fraction is $(1-P_{FTR})$. For the case of multiple true target types, the dimensions of the matrix will be higher; however, for this research only a 2×2 matrix is considered and shown in Table 1.

Ideally it is preferred to have $P_{TR}=1$ and $P_{FTR}=1$, that is, the confusion matrix is an identity matrix, or at least diagonally dominant. ATR is far from achieving this goal, and in general $0<P_{TR}<1$ and $0<P_{FTR}<1$. These parameters are crucial in determining the effectiveness of an autonomous weapon or surveillance system, and are typically determined through extensive captive testing of the Sensor/ATR subsystem.

In general, a false target may be able to mislead an ATR algorithm into believing and recognizing it as a true target. For a single warhead munition, the probability of recognizing the true target in the incremental area ΔA is conditioned on not having declared a true target prior to arriving at ΔA. Thus the incremental probability of encountering a target in ΔA is

$$\Delta P_E = P_{\overline{FTR}}(A)\frac{\Delta A}{A_S} \tag{20}$$

where $\frac{\Delta A}{A_S}$ is the probability that a true target is in ΔA and $P_{\overline{FTR}}(A)$ is the probability of both true and false recognitions while searching the area A leading up to ΔA.

The probability of no false target recognitions while searching area A, denoted by $P_{\overline{FTR}}(A)$ can be approximated by summing the probabilities of 0, 1, or many false target encounters that do not result in an incorrect target declaration [13].

$$P_{\overline{FTR}}(A) = e^{-\alpha A} + P_{FTR} e^{-\alpha A} \frac{(\alpha A)}{1} + P^2{}_{FTR} e^{-\alpha A} \frac{(\alpha A)^2}{2} + \ldots$$

Hence, $$P_{\overline{FTR}}(A) = e^{-\alpha A} + \sum_{k=1}^{\infty} P^k{}_{FTR} e^{-\alpha A} \frac{(\alpha A)^k}{k!}$$

$$= \sum_{k=0}^{\infty} P^k{}_{FTR} e^{-\alpha A} \frac{(\alpha A)^k}{k!}$$

$$= e^{-\alpha A} \sum_{k=0}^{\infty} P^k{}_{FTR} \frac{(\alpha A)^k}{k!}$$

$$= e^{-\alpha A} \sum_{k=0}^{\infty} \frac{(P^k{}_{FTR} \alpha A)^k}{k!}$$

$$= e^{-\alpha A} e^{P_{FTR} \alpha A}$$

$$= e^{-(1-P_{FTR})\alpha A}$$

Now consider that the battle space consists of a Poisson field of targets, parameterized by λ_T, and a Poisson field of false targets, parameterized by λ_{FT}. Let *t* be the time of a true target attack. The probability density function of the random variable *t* is [13],

$$f(t) = e^{-(1-P_{FTR})\lambda_{FT}\frac{t}{T}} e^{-P_{TR}\lambda_T\frac{t}{T}} \frac{1}{T}\lambda_T P_{TR} \tag{21}$$

That is,

$$f(t) = \frac{1}{T} P_{TR}\lambda_T e^{-[(1-P_{FTR})\lambda_{FT}+P_{TR}\lambda_T]\frac{t}{T}} \tag{22}$$

Let τ be the time of a false target attack. By symmetry, the probability density function of a random variable τ is

$$g(\tau) = \frac{1}{T}(1-P_{FTR})\lambda_{FT} e^{-[(1-P_{FTR})\lambda_{FT}+P_{TR}\lambda_T]\frac{t}{T}} \tag{23}$$

Finally the probability of a true or a false target attack not happening at some time $\tilde{T}$, is

$$H(s) = e^{-[(1-P_{FTR})\lambda_{FT}+P_{TR}\lambda_T]\frac{\tilde{T}}{T}} \tag{24}$$

Thus the respective probabilities for a true and a false target attack have been derived as:

$$P_{A_T} = \frac{P_{TR}\lambda_T}{(1-P_{FTR})\lambda_{FT} + P_{TR}\lambda_T}\{1-e^{-[(1-P_{FTR})\lambda_{FT}+P_{TR}\lambda_T]}\} \tag{25}$$

$$P_{A_{FT}} = \frac{(1-P_{FTR})\lambda_{FT}}{(1-P_{FTR})\lambda_{FT} + P_{TR}\lambda_T}\{1-e^{-[(1-P_{FTR})\lambda_{FT}+P_{TR}\lambda_T]}\} \tag{26}$$

Note that for the single munition, single target scenario,

$$P_{A_T} = P_{A_{FT}} \Leftrightarrow P_{TR}\lambda_{FT} = (1-P_{FTR})\lambda_{FT},$$

and

$$P_{A_T} + P_{A_{FT}} = 1-e^{-[(1-P_{FTR})\lambda_{FT}+P_{TR}\lambda_T]}.$$

Expected Values for True and False Target Attacks. For the case of a wide area search vehicles with multiple bombs, Decker derived equations to estimate numbers of true and false target attacks [14], which are shown below for reference. For the case of Poisson distributions, the probability of specified number of true target attacks is,

$$\begin{aligned} P_t^{(w)}\ (A_s) = \lambda_{AT}^t \lambda_{AFT}^{(w-t)} \frac{w}{t!(w-t)!}\int_0^1 \{e^{-(\lambda_{AT}+\lambda_{AFT})^x} x^{w-1}\}dx + \\ \sum_{f=0}^{w-t-1} e^{-(\lambda_{AT}+\lambda_{AFT})}\ \lambda_{AT}^t \lambda_{AFT}^f \frac{1}{t!f!} \end{aligned} \tag{27}$$

The expected number of true targets attacks, $E[t]$ is

$$E[t]=\sum_{t=0}^{w} tP_t^{(w)}(A_s)$$

$$E[t]=\sum_{t=0}^{w} t\frac{\lambda_{AT}^{t}\lambda_{AFT}^{(w-t)}}{(\lambda_{AT}+\lambda_{AFT})^{w}}\binom{w}{t}\frac{\gamma(w,(\lambda_{AT}+\lambda_{AFT})x)}{\Gamma(w)}+ \sum_{t=0}^{w-1}\sum_{f=0}^{w-t-1} t\frac{(\lambda_{AT}x)^{t}}{t!}\frac{(\lambda_{AFT}x)^{f}}{f!}e^{-(\lambda_{AT}+\lambda_{AFT})x} \tag{28}$$

where Γ and γ represent the gamma and incomplete gamma functions, respectively.

The probability of specified number of false target attacks is,

$$P_{(\cdot),f}^{(w)}(A_s)=\frac{\lambda_{AT}^{w-f}\lambda_{AFT}^{f}}{(\lambda_{AT}+\lambda_{AFT})^{w}}\binom{w}{f}\frac{\gamma(w,(\lambda_{AT}+\lambda_{AFT})x)}{\Gamma(w)}+ \sum_{t=0}^{w-f-1}\frac{(\lambda_{AT}x)^{t}}{t!}\frac{(\lambda_{AFT}x)^{f}}{f!}e^{-(\lambda_{AT}+\lambda_{AFT})x} \tag{29}$$

and the expected number of false targets attacks, $E[f]$ is

$$E[f]=\sum_{f=0}^{w} f\frac{\lambda_{AT}^{w-f}\lambda_{AFT}^{f}}{(\lambda_{AT}+\lambda_{AFT})^{w}}\binom{w}{f}\frac{\gamma(w,(\lambda_{AT}+\lambda_{AFT})x)}{\Gamma(w)}+ \sum_{f=0}^{w-1}\sum_{t=0}^{w-f-1} f\frac{(\lambda_{AT}x)^{t}}{t!}\frac{(\lambda_{AFT}x)^{f}}{f!}e^{-(\lambda_{AT}+\lambda_{AFT})x} \tag{30}$$

Note that for the case of $x = 1$, where the whole battle space is searched, and a large number of bombs is available ($w \to \infty$), we get $E[t] \to \lambda_{A_T}$ and $E[f] \to \lambda_{A_{FT}}$.

The ROC curve

The Receiver Operating Characteristic (ROC) curve is illustrated in Figure (8). By tradition, the plot shows the false positive rate on the *x* axis and true positive rate on the *y* axis.

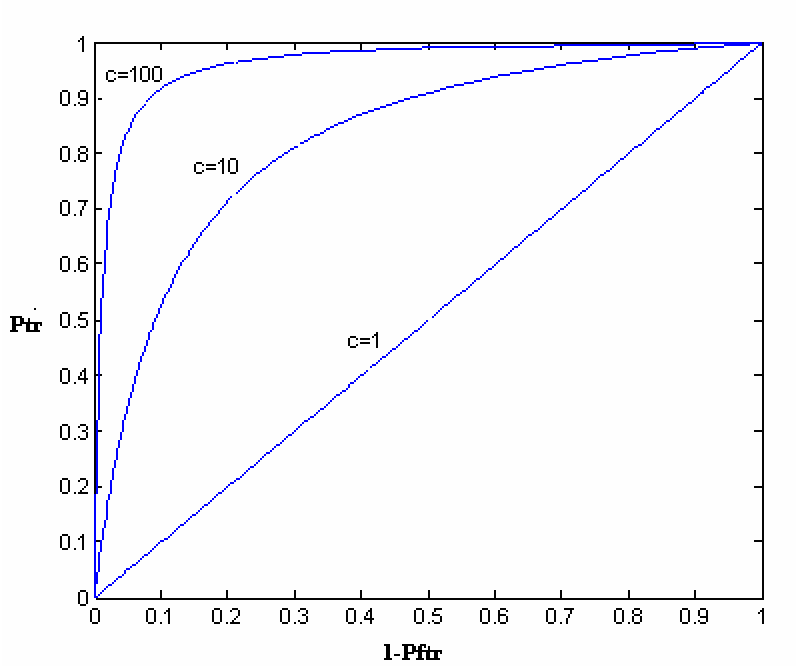

Figure 8. Receiver Operating Characteristic curve

The ROC curve is a graphical representation of the trade off between the true and false positive rates for varying sensor thresholds. Equivalently, the ROC curve is the representation of the trade offs between sensitivity and specificity (any increase in sensitivity will be accompanied by a decrease in specificity). The ROC curve demonstrates several things:

1. The closer the curve follows the left-hand border and then the top border of the ROC space, the more accurate sensor ATR algorithm it depicts.

2. The closer the curve comes to the 45-degree diagonal of the ROC space, the less accurate the test.

3. The slope of the tangent line at a cut point gives the likelihood ratio for that value of the test.

4. The area under the curve is a measure of test accuracy. While an area of 1 will give an excellent result, as the area decreases the accuracy of the result will be degraded.

The parameters P_{TR} and P_{FTR} introduced earlier are dependent on each other and characterize the sensor's performance. With these two parameters the ROC curve is developed to show the relationship between them. An empirical equation for an experimentally determined ROC curve is defined by [15, 16]:

$$1-P_{FTR}=\frac{P_{TR}}{(1-c)P_{TR}+c} \tag{31}$$

The ROC parameter, c, will depend on the area search rate, and pixel density. It also depends on the sensor and data processing algorithms, and the characteristic size of the target. How well a sensor detects and recognizes a given target depends on how well it sees it; that is, how many pixels are on the target. The greater the number of pixels the sensor has on the target the better it can see it. The number of pixels on target depends on how large the target is, and how many pixels the sensor is capable of delivering and processing in the given time.

For simplicity, it can be said that the ROC parameter is,

$$c = f\left(\frac{P_t \cdot l_t}{w \cdot V}\right) \tag{32}$$

A general observation is that the faster the area search rate is; lower the value of the ROC parameter. Intuitively it is seen that the faster the vehicle, the bigger the sensor footprint will be for a given time length, and the more targets it is likely to encounter. Since the vehicle is now moving faster, it has less time to process the target information so it is more likely to make erroneous declarations.

A parameter, $k\overline{c}$ can be defined that will make c dimensionless.

Let
$$k\overline{c} \equiv \frac{c \cdot w \cdot V}{P_t \cdot l_t}$$

Similarly, define a parameter,
$$\hat{c} \equiv \frac{c}{k\overline{c}} \tag{33}$$

Equation (33) is a simplified version of equation (32) derived for the purpose of ease to work with when using dimensional analysis.

Summary

In this chapter, the independent parameters that define a basic wide area search vehicle were identified and the target recognition and attack algorithms for a Poisson distribution of targets in a rectangular battle space were set up. Having identified these design variables and their relationships to each other; it is now possible to apply the Buckingham Pi theorem to non-dimensionalize these parameters in order to explore possibilities of scaling.

III. Application of Buckingham Pi theorem

Introduction to Buckingham Pi Theorem

The ability to compare scaled experiments to full sized experiments depends primarily on the concept of dynamic similitude. Two systems of different size will be "dynamically similar" if the governing differential equations are identical after accounting for dimensional scaling of each parameter in the equation.

The Buckingham Pi theorem [17] states that the solution to any differential equation, regardless of its order or nonlinearity, can be made invariant with respect to dimensional scaling as long as appropriate ratios of parameters are maintained. This is shown via non-dimensionalizing the independent dimensional parameters. If two systems are modeled by the same differential equations and have the same Π groups, then the systems are dynamically similar.

Consider a physically meaningful equation given in the form of,

$$f(q_1, q_2, q_3, ..., q_n) = 0$$

where q_i are the n are physical variables expressed in terms of k independent physical units. Then the above equation can be written as,

$$F(\Pi_1, \Pi_2, \Pi_3, ..., \Pi_n) = 0$$

where the Π_i are dimensionless parameters constructed from the q_i by

$p = n - k$ equations in the form of

$$\Pi_i = q_1^{m_1} q_2^{m_2} q_3^{m_3} ... q_n^{m_n}$$

The exponents m_i are rational numbers. Application of the Pi theorem for the research problem is as follows:

From equations (1) to (7), (11) and equation (33) derived in the previous chapters it can be seen that the vehicle and sensor dynamics can be represented by the following independent variables:

$d, V, g, w, \hat{c}, \rho_T, z, l_t, O_L$

Therefore the number of variables,

$$n = 9$$

The fundamental dimensions of these variables are length [L] and time [T]. So,

$$k = 2$$

By Buckingham's Theorem, the number of dimensionless equations (Π groups) is,

$$p = n - k = 9 - 2 = 7$$

We select a recurring set that contain two variables that cannot by themselves form a dimensionless group. Thus, we select the two variables d and V.

The dimensions of these variables are:

$$d = [L]$$

$$V = [L][T^{-1}]$$

Rewriting the dimensions in the terms of the variables chosen,

$$[L] = d$$

$$[T] = dV^{-1}$$

Dimensionless groups are formed by taking g, w, z, $\hat{c}$, ρ_T, l_t, O_L in turn:

The footprint length, z has dimensions of $[L]$, therefore $z \cdot [L^{-1}]$ is dimensionless. Thus a pi group can be formed as,

$$\Pi_1 = z / d$$

Similarly taking the footprint width into consideration,

$$\Pi_2 = w / d$$

From Equation (7), g has dimensions of $[L][T^{-2}]$, therefore $g \cdot [L^{-1}][T^2]$ is dimensionless. Therefore,

$$\Pi_3 = g \cdot (1/d) \cdot (d^2 / V^2)$$

$$\Pi_3 = g \cdot (d / V^2)$$

From Equations (32) and (33), $\hat{c}$ has dimensions of $[L^{-1}][T]$, therefore $\hat{c} \cdot [L][T^{-1}]$ is dimensionless, and forms the pi group,

$$\Pi_4 = \hat{c} \cdot [L][T^{-1}]$$

$$\Pi_4 = \hat{c} \cdot V$$

From Equation (6), ρ_T has dimensions of $[L^{-2}]$, therefore $\rho_T [L^2]$ is dimensionless, and forms the pi group,

$$\Pi_5 = \rho_T d^2$$

Consider a target that the vehicle might encounter, having a characteristic target length l_t that has dimensions of $[L]$. Then $l_t [L^{-1}]$ is a dimensionless quantity,

$$\Pi_6 = \frac{l_t}{d}$$

Frame overlap, O_L has units of $[L]$, therefore $O_L[L^{-1}]$ is a dimensionless quantity,

$$\Pi_7 = \frac{O_L}{d}$$

Physical Relevance of the Pi Groups

When working with actual systems, scaling factors can be developed as follows:

$$scale = \frac{\langle \Pi_i \rangle_{GUESS}}{\Pi_i}.$$

The term $\langle \Pi_i \rangle_{GUESS}$ denotes a guessed pi value for the full scale model, and Π_i denotes the nominal pi group value. The scaling factor, which is the ratio between these values could be utilized with the definitions of the Πs to determine the actual parameters of the concept vehicle.

In order to have a constant (or a range of) characteristic length that the sensor could observe for a given vehicle operating under different speeds, lets define that for the nominal case a target with a length of 10 meters could be detected with its sensor. Therefore, in this case the target length to footprint ratio will differ as speed is changing. From this, it is possible to determine the ROC curve the vehicle will have to fall on in order to detect this target, and also how the pixel density changes with speed. Velocity and g limit are limiting factors of the vehicle whereas l_t is a limiting factor of the sensor and the vehicle.

The Buckingham Pi theorem states that if two vehicles are described by the same differential equations, then the solutions of the differential equation for both vehicles will be the same if the Π groups are the same. By establishing that two systems have dynamic similitude, we can then say that one vehicle could be defined in terms of the other by some scale factor. If the Π groups match, and both systems are governed by the same set of dynamic and imaging principles, then the normalized pole locations will be the same [4]. Thus, a high degree of dynamic similitude between the vehicles will require the two systems to have the same characteristic equation.

It is required to compare the Π values of the concept vehicle to a distribution of Π values of real vehicles to see how well the comparison is. Then we can see how the Π groups change, and in fact similitude can be achieved in order to see the possibilities of scaling.

The Vehicles

In order to analyze the pi groups and their relationship to the actual vehicle performance characteristics, numerical calculations were carried out for 3 types of scenarios in order to observe the variation of various parameters under a velocity range.

The Nominal Vehicle. For this purpose, the nominal case was considered to be an aircraft, whose average performance was a velocity of 125 meters/sec and a *g* limit of 2, having a Low Cost Autonomous Attack System with a Laser Radar based guidance (LOCAAS LADAR) sensor mounted on it. It should be noted that the nominal vehicle is user defined for the particular experiment, depending on the requirements. All comparisons drawn will be relative to this selection; hence, it should be a vehicle whose characteristics are well defined and known.

The Slow Surrogate Vehicle. The 1/20 scaled Tamiya Mammoth Dump truck, was chosen as the slower moving vehicle in experiment, since it could be considered to be a possible surrogate for future hardware experimentation in this area. The dump truck is capable of moving at a velocity of 1.5 meters/sec and has an approximate turn radius of 4.7 meters.

Figure 9. Tamiya 1/20 Mammoth Dump Truck

The Fast Surrogate Vehicle. The Chinese built K-8 jet trainer, with an average performance of 275 meters/sec and -3/7 g's, was chosen as the faster moving subject. However, this vehicle would not be an ideal vehicle to perform an actual experiment of this nature. It was chosen for the purpose of drawing comparisons for this research.

Figure 10. K-8 Jet Trainer

The following table gives the available data for the subject vehicles. From these values, it is possible to calculate the values of the nominal pi groups, and draw comparisons between the two subject vehicles.

Table 2. Design Parameters and Performance for the Straight Search Scenario of the Subject vehicles

Vehicle/Sensor Parameter	Nominal Vehicle	1/20 Dump Truck	K-8 Jet Trainer
Velocity (V) m/sec	125	1.5	275
g limit m/sec^2	2	0.05	3-5

Normal Operating Altitude of the Sensor (h) meters	250	1	2500
Frame Overlap(O_L) meters	50	N/A	N/A
Pixel Density (ρ) pixels/m^2	10-15	N/A	N/A
Dead Range of the sensor (d) meters	1000	N/A	N/A
Footprint Width (w) meters	500	N/A	N/A
Footprint Length (z) meters	200	N/A	N/A
Swath Angle (Θ) degrees	20	N/A	N/A
VFOV degrees	4.039	N/A	N/A
Desired Target Characteristic Length (l_t) meters	10	0.1	20

Development of Pi groups

By comparison of known data of the subject vehicles, the following distribution of pi groups can be obtained. Looking at the individual pi groups for the nominal vehicle,

Pi Group 1. The first pi group is the ratio of footprint length to dead distance as shown in Equation (34). It represents the normalized elevation field of regard.

$$\Pi_1 = \frac{z}{d} = 0.2 \tag{34}$$

It shows that the dead range and foot print length are proportional to each other. If dead range is decreased or increased, the footprint length will decrease or increase respectively by a factor of 0.2 based on the pi groups calculated for this case. That is, if the sensor is looking down at a closer distance away from its location, its footprint will have less length than when it was looking further away. This is also made obvious by the fact that VFOV increases with velocity (turn rate), since higher VFOV delivers a larger (lengthier) and a more "spread out" footprint.

Pi Group 2. The second pi group is the ratio of footprint width to dead range. It represents the normalized azimuthal field of regard.

$$\Pi_2 = \frac{w}{d} = 0.5 \tag{35}$$

For a given swath angle, the closer the sensor looks down (smaller *d*) the smaller the width that it will be looking at. Since *d* and *w* are proportional to each other, if the dead range is decreased by 1 unit, then the sensor looks down closer, and the width of the footprint would be decreased by a factor of 0.5. The closer the sensor looks down, the smaller the area of the footprint will be. It should be noted that since for this research swath angle is held constant this will always be true.

Pi Group 3. This is the most critical pi group, since it is the key to defining the type of vehicle that is taken into consideration. For this research, velocity and turn rate are the sole parameters that defined each vehicle.

$$\Pi_3 = g\frac{d}{V^2} = 1.254 \quad (36)$$

Equation (36) can also be written as

$$\Pi_3 = \frac{d}{r} = 1.254\,, \quad (36a)$$

which makes it the ratio of turn radius to dead range. This shows that *d* and *r* are proportional to each other. But since $r = \dfrac{V^2}{G \cdot g}$, then V^2, *r*, and *d* are proportional to each other. For a vehicle operating at a slower velocity (like the dump truck), having a smaller radius of turn, with a constrained *g* limit, the sensor looks out closer, resulting in a smaller dead range. This pi group gives a feel of how fast (or slow) a vehicle should move in order to capture an object within the sensor footprint. For a closer object the vehicle can, at a given velocity, make a sharper turn; or, for a given turn rate, increase the velocity and turn at a smaller radius, thereby reducing the dead range. For a far off object, the vehicle does not have to make rapid maneuvers to make and engagement.

For the purpose of calculations in this research, for a selected operating velocity range, a possible turn rate is defined (which will be a characteristic unique for each vehicle). There by it is possible to calculate the dead range when the velocity and turn rate is known. Now that the dead range is known, it is possible to calculate the footprint width and length and pixel density.

Pi Group 4. The fourth pi group is given by Equation (37) below.

$$\Pi_4 = \hat{c} \cdot V = 200000 \quad (37)$$

The velocity that the vehicle is flying at, the area search rate of the vehicle, and the quality of the image (resolution) will determine which ROC curve the vehicle will be on.

Note that $\hat{c} = \dfrac{c}{k\overline{c}} = \dfrac{l_t \cdot P_t}{w \cdot V}$. For the nominal case, the vehicle is on a ROC curve where c =100 and $k\overline{c}$ =0.0625. The parameter $k\overline{c}$ is a constant that will differ depending on the "nominal case" defined for the experiment. It is seen from the graphs that the higher the speed and maneuverability of the vehicle the lower the ROC parameter will be; hence, it will be on a lower ROC curve. A vehicle yielding a higher area search rate may be constrained to deliver a lower pixel density in order to keep in pace with the processing limitations of a given image. Thus, if the pixel density is held constant it will require having higher processing rates in order to capture and recognize the target in the time available. Since the jet trainer is closer in performance to the nominal vehicle, it will be flying on the ROC curve of c = 45.5, whereas the dump truck, which has a much smaller turn radius than the nominal case, will have to be on a much higher ROC curve (c= 8333.33) to achieve the same sensor performance characteristics.

Pi Group 5. The number of pixels the sensor is capable of generating for any given footprint is given by the fifth pi group.

$$\Pi_5 = \rho_T \cdot d^2 = 10^7 \tag{38}$$

Equation (38) gives a feel of how the pixel density changes as the sensor captures far-off objects. Note that for a given sensor the number of pixels per foot print remains a constant. Hence, the larger the area of the sensor footprint the smaller the pixel density will be. The further away the sensor looks, the larger the footprint will be, and the poorer the resolution. For a case like the dump truck, where the sensor is looking at a much smaller area in close vicinity, we would have a very high pixel density and a very clear image if the target is large enough to make use of the available pixels. In such cases, a very small fraction of the available pixels is sufficient to recognize an object and therefore it is unnecessary to process all the incoming information. Thus, we can have higher processing speeds, whereas for a vehicle flying at a much higher velocity like the jet trainer, will be looking at a much larger footprint area and will need to process all the incoming information before it can make a proper recognition of the image that it captured.

Going back to the confusion matrix, it could be said that for a slower moving vehicle, P_{TR} will be higher whereas for a vehicle moving at higher speed P_{FTR} will be higher.

Pi Group 6. This is the ratio of the footprint length to the target characteristic length.

$$\Pi_6 = \frac{l_t}{d} = 0.01 \tag{39}$$

This pi group will enable us to see what size range of targets the vehicle would be capable of detecting with the given sensor and speed, and which ROC curve it should be flying on in order to obtain optimal results for given target sizes.

Pi Group 7. The seventh pi group gives the ratio of footprint overlap to dead range .

$$\Pi_7 = \frac{O_L}{d} = 0.05 \qquad (40)$$

This pi group gives a feel of how much overlap the sensor should generate within its footprints so that it can have a target within its area of vision as speed increases or decreases. For the purpose of simulation, the percentage of frame overlap ($\frac{O_L}{z}\%$) will be considered. For the nominal case, overlap is 50 meters, which is 25% of the total footprint length.

For easy reference the pi values obtained for the nominal vehicle are listed in Table 3. It should be noted that the values of the pi groups will vary depending on what vehicle is considered to be nominal.

Table 3. Pi Values for the Nominal Vehicle

Pi group	Value
Π_1	0.2
Π_2	0.5
Π_3	1.254
Π_4	200000
Π_5	10^7
Π_6	0.01
Π_7	0.05

Parameter Variation

The variation of vehicle and sensor parameters, as well as footprint parameters are depicted in Annex A for the nominal and subject vehicles and varying turn rate and characteristic target length. From the results obtained, it is seen that as vehicle speed (turn radius) increases the sensor footprint size, frame overlap and detectable target size have a linear increment. On the other hand, pixel density, and ROC parameter value, show rapid decay. The search swath angle remains constant, while the depression angle and VFOV increase. The same trends were seen as target characteristic length was increased for all the above parameters. Here, the nominal case was compared to the different types of vehicles and the distribution of the pi groups as each aircraft acted as a surrogate for the nominal sensor observed

Calculations were also carried out by replacing the nominal sensor with a digital camera, and considering the dump truck as the nominal vehicle. Here while the pi groups remained the same, their values changed. The variation of parameters for this scenario was observed to have the same trends as before and the angles in consideration (swath angle, VFOV, and depression angle) remained within acceptable limits.

Summary

In this chapter we were able to apply dimensional analysis for the vehicle and sensor performance parameters and derive seven pi groups. The significance of each pi group was discussed. The variation of desirable parameter values were observed for a range of velocity and target sizes. It was seen that as vehicle speed increases the area that the sensor will be looking at will increase. This rate of increment (of area search rate) depends on how fast the vehicle is flying and how fast it can turn. It was seen that for a smaller vehicle as the dump truck, the pixels on target will be very high since the sensor is looking at a much smaller area. Since now the sensor has a high resolution image, it is easier to identify the target. Hence, it would have a lower false target recognition rate, and it will fall on a high ROC curve. The VFOV, azimuthal, and vertical angles of view of the sensor, for each of the cases were found to be within its acceptable ranges.

IV. Simulation

Simulation

General. A MATLAB program was developed to simulate the vehicle travel, foot print development, target distribution, identification, declaration and attack. This code models two configurations: (1) Known Vehicle Velocity and *g* limit (minimum turn rate), and (2) Known Target Size and *g* limit. In both configurations the specifications for the nominal (real world) vehicle are entered. The difference between the two configurations is in the input and output parameters for the experimental/surrogate vehicle. The surrogate vehicle inputs for the first configuration are vehicle velocity, g limit and altitude, and for the second configuration are desired target characteristic length, g limit and altitude. The program returns the remaining parameters for the surrogate as outputs. The program serves as a basis for comparisons between different vehicles under varying performance parameters and conditions. The simulated vehicle is capable of flying in two modes: straight search mode and attack mode.

Option 1- Known Velocity and g limit

Development of the Pi Groups. The code was developed such that the user can choose the option under which the vehicle initially operates, i.e., if it is made to operate at a known velocity and g limit (known minimum turn radius), or made to observe a target of predefined size. The pi groups were developed per the nominal case.

While the pi groups will always remain the same for the parameters considered, their values will change depending on what is selected to be the "nominal" vehicle.

For this research, the nominal case was always considered to be the wide area search vehicle having a performance capability of 125 meters/sec and 2 g's. The nominal pi groups will then be compared to the pi groups of each of the individual subjects so that desired vehicle and sensor parameters can be calculated. The surrogate vehicles were the dump truck and the jet trainer as described in the previous chapter. Consider for example the case where the dump truck was the surrogate, where the input variables are velocity (1.5 m/sec) and *g* limit (1.5 m/sec ^{2}). The desired vehicle parameters are calculated as illustrated below, using the pi values obtained from the nominal vehicle in Table 3:

From equation (36) dead range,

$$d = \frac{\Pi_3 \cdot V^2}{g} = 5.76 \text{ meters}$$

From equation (34) frame length,

$$z = \Pi_1 \cdot d = 1.152 \text{ meters}$$

From equation (35) frame width,

$$w = \Pi_2 \cdot d = 2.88 \text{ meters}$$

From equations (32) and (37) ROC parameter,

$$c = \frac{\Pi_4 \cdot k\overline{c}}{V} = 8333$$

From equation (38) pixel density,

$$\rho_T = \frac{\Pi_5}{d^2} = 301408 \text{ pixels/m}^2$$

From equation (39) characteristic target length,

$$l_t = \Pi_6 \cdot d = 0.0576 \text{ meters}$$

From equation (40) frame overlap,

$$O_L = \Pi_7 \cdot d = 0.288 \text{ meters}$$

It was found that as the vehicle turn radius increased the size of the footprint and search rate also increased. The larger footprint means the vehicle would be capable of looking at larger targets; however, the number of pixels on target was degraded, thereby making it more difficult for the sensor to recognize the targets since it had less information and less time to process the available information.

Target placement. A true and false target matrix was randomly distributed in the area the vehicle covers during its travel. The length of the distribution on the *x* and *y* axes is a function of the footprint width and total distance traveled by the vehicle, respectively. The targets have a random position and a random true or false target assignment based on the number of targets. Additionally, each target is assigned a random target length based on the characteristic target length it should have (based on the pi group calculations). The number of targets will depend on the probability distribution used, which for this case is a Poisson probability distribution approximated by a uniform distribution.

For the dump truck the area of the battle space,

$$A_s = w \cdot X_S \cdot D \cdot Y_S \tag{41}$$

where D is the total distance traveled and X_S is the x scale and Y_S is the y scale. The total distance that the vehicle would ideally travel in the time duration of mission (T = 10 minutes for this experiment) is the length of the battle space. The number of time steps the simulation would run is a function of V and desired O_L and can be calculated as,

$$\delta t = \frac{z - O_L}{V}$$

$$= 0.576 \text{ seconds.}$$

Total distance (D) the vehicle would travel if no targets are encountered,

$$D = V \cdot T$$

$$= 900 \text{ meters}$$

Then from Equation (41), the area of the battle space of the dump truck for the given time duration,

$$A_s = 7776 \text{ meters}^2$$

Total area covered by the sensor in search mode,

$$A = w \cdot V \cdot T$$

$$= 2592 \text{ meters}^2$$

The x scale was 3 units and the y scale was 1 unit. Note that the area covered by the sensor,

$$A = A_S \cdot \frac{Y_S}{X_S}$$

From equations (14) and (15) the number of true targets (NT) and false targets (NFT) will be

$$NT = \lambda_T \frac{A_s}{A} = 15$$

$$NFT = \lambda_{FT} \frac{A_s}{A} = 30$$

where the expected number of true targets, $\lambda_T = 5$ and the expected number of false targets, $\lambda_{FT} = 10$.

Target Detection and Declaration. Once the vehicle starts moving it is able to search an area which has dimensions of the footprint, calculated by means of the pi groups. At this point a selection could be made as to whether the vehicle will fly straight and level or not (in which case the turn radius will be purely a function of the velocity and *g* limit).

As the vehicle footprint passes over each target it will keep track of the number of detections it makes. If the target delivers sufficient pixels, such that identification could be made, the declaration algorithm will make a declaration based on the ROC curve. An attack is made if a target is declared to be true (regardless of whether or not the declaration is correct), thereby increasing the number of true or false target attacks. If there is more than one true declaration in the same footprint, a decision is made to attack the target that was detected first. In the case where a target does not provide sufficient image quality to make a correct identification, the vehicle gives a message that the target cannot be seen clearly. The declarations are purely based on the ROC curve; hence, the selection of the nominal case for each experiment is vital since it will have an impact on the comparative ROC values of the subjects.

Target Attacks. Once a target is seen and declared to be true, the vehicle will switch from search mode to attack mode in order to perform the attack function. The vehicle will start moving toward the target on a path whose length and time to traverse is based on the vehicle's velocity, maximum maneuver capability, and the position of the target in its footprint.

The number of attacks made is based on how many true declarations are made; hence, the number of true target attacks (NTA) and false target attacks (NFTA) is based on the statistical properties of the simulation that determines the number of targets, their truth assignment, and the detection and declaration algorithm. The munition can be assigned some value of lethality and its capability of destroying an attacked target can be measured. This is achieved in the simulation by a random draw and a probability of kill (P_K). When an attack is made, a comparison is made with the value of P_K by conducting a random draw, and based on this factor it is decided whether the hit was a success or not. Accordingly the target would be declared to be killed or not killed. There are two types of non-lethal attacks: missed targets and low lethality warheads. There would be missed targets in the case where the vehicle did not have a maneuvering capability sufficient to reach the target in the given time. In other words, the vehicle would not have a small enough minimum turn radius.

Figure (11) illustrates the aircraft traversing toward the target to perform an attack.

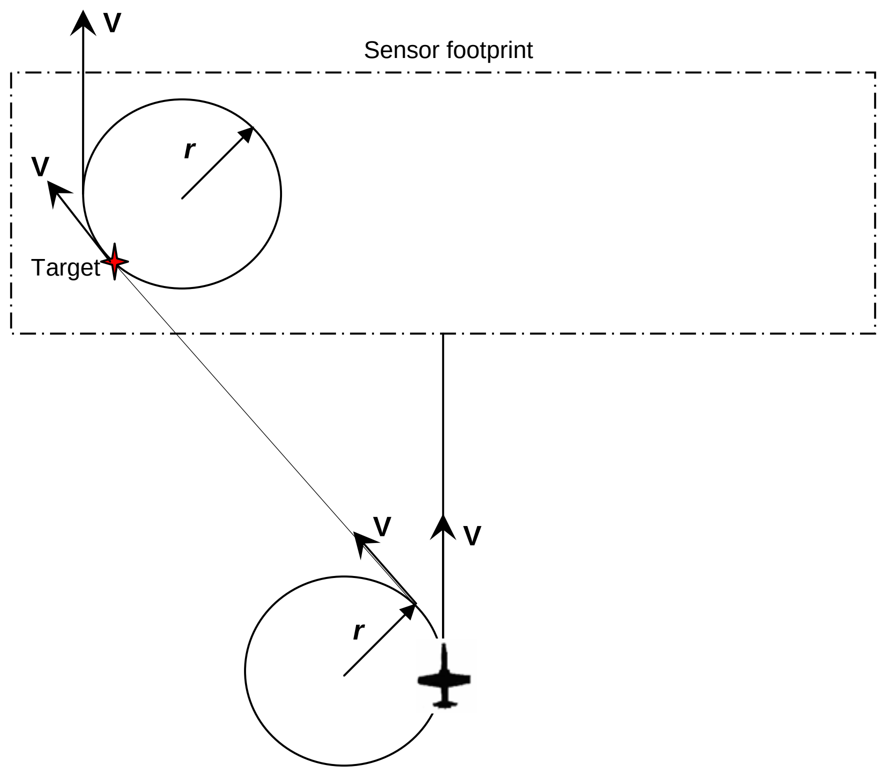

Figure 11. Aircraft in Attack Mode

Figure (12) shows a snap shot of the simulation in progress where the vehicle is generating footprints ahead of its position, detecting the targets, making maneuvers to engage recognized targets and then continuing the search. Note that in this simulation, the search is always conducted in the north (straight up) direction. The true targets are shown by star symbols and the false targets are shown by crosses.

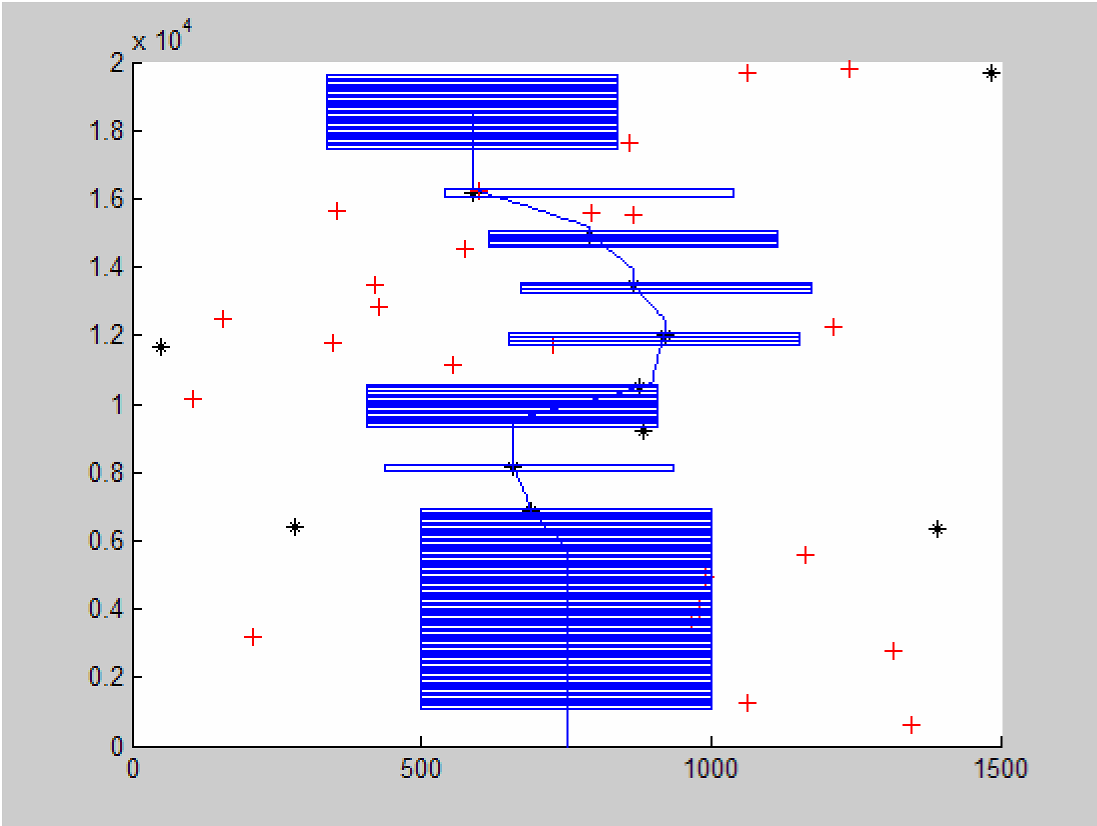

Figure 12. Snap shot of Target Search and Attack Simulation

Flow Chart of the Simulation

The basic logic of the simulation is depicted in the flow chart in Figure (13) below.

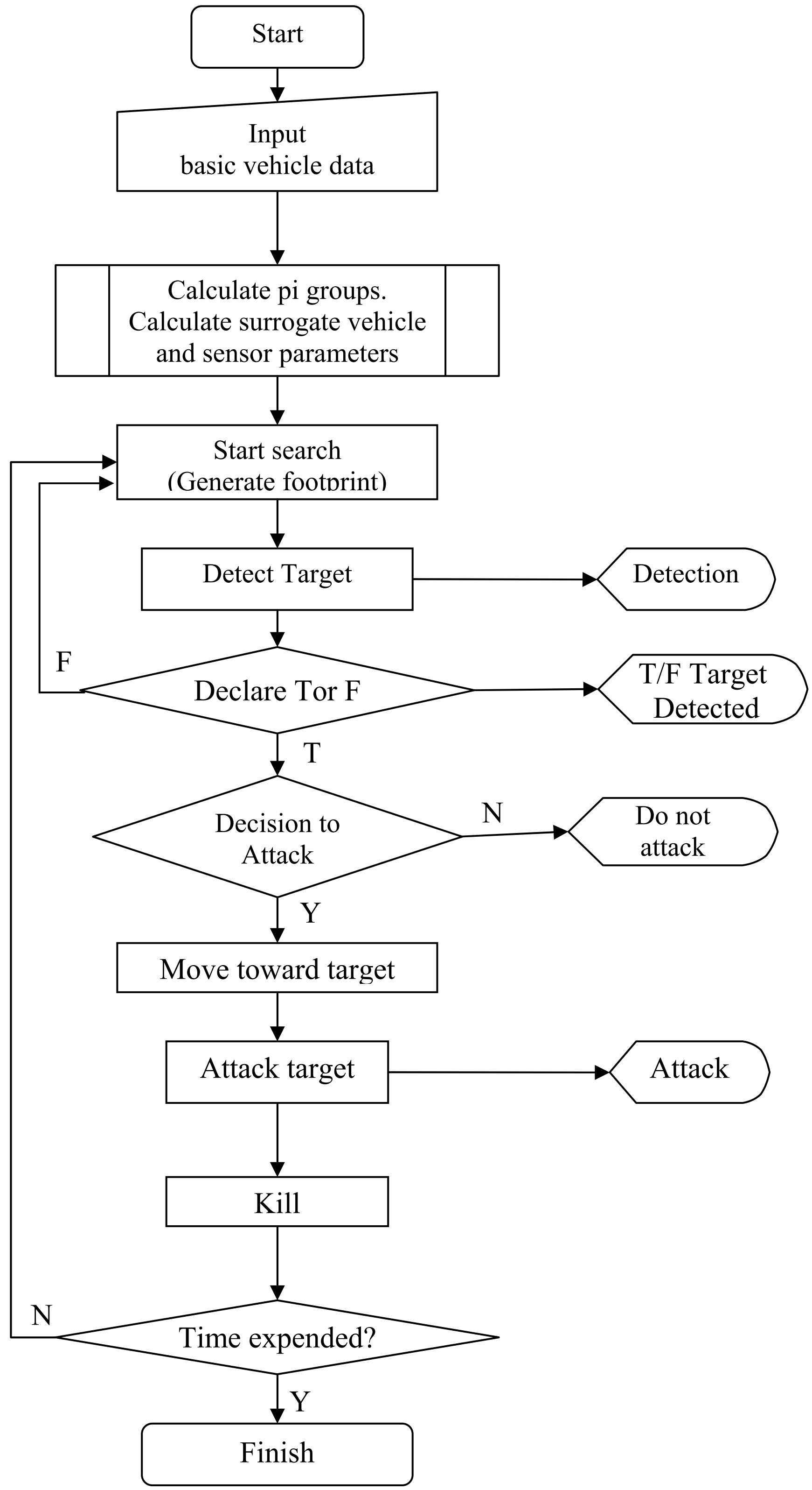

Figure 13. Flow Chart of Simulation

Option 2- Known Target size

In the case where the vehicle is tasked to look at a target with predefined size, the MATLAB code will calculate the desired turn radius of the vehicle in order to engage the targets. It was seen that the increase in the desired target size to be detected had the same effects on the results as increasing the turn radius. This is evident in the results given in Appendices A and B.

Below is an example illustrated in terms of the dump truck of how the results are in cohesion with option 1. The input parameters are desired characteristic length (chosen to be 0.0576 meters) and *g* limit (0.05 meters/sec^2).

The dead range,

$$d = \frac{l_t}{\Pi_6} = 5.76 \text{ meters}$$

Senor footprint length,

$$z = \Pi_1 \cdot d = 1.152 \text{ meters}$$

Senor footprint length,

$$w = \Pi_2 \cdot d = 2.88 \text{ meters}$$

Turn radius,

$$r = \frac{d}{\Pi_3} = 4.5871 \text{ meters}$$

Vehicle velocity,

$$\mathrm{V}=\sqrt{\mathrm{g} \cdot 9.81 \cdot \mathrm{r}} = 1.5 \text{ meters. /sec}$$

ROC parameter,

$$c = \frac{\Pi_4 k\overline{c}}{V} = 8333$$

Pixel density,

$$\rho_T = \frac{\Pi_5}{d^2} = 301408 \text{ pixels/m}^2$$

Frame overlap,

$$O_L = \Pi_7 \cdot d = 0.288 \text{ meters.}$$

The target matrix will randomly distribute targets with a constant characteristic length; therefore, when the vehicle passes over the target it is bound to be detected as it will always deliver the same number of pixels on target. The declaration will then be made, as before, according to the ROC curve. The importance of having this option is that it would be much easier to have a predetermined range of target sizes to carry out an actual hardware experiment than varying the turn radius of an available test vehicle.

The Random Draw and Variance Reduction

When running multiple instances of the simulation for a given scenario (for a particular vehicle), the algorithm, and set performance parameters will be the same. Only the randomness of the environment will differ. Due to this fact, the output of the simulation will have a variance, which for a given experiment will cause confusion as to whether the change in the characteristics and results of the wide area search vehicle is due to the factors under test or random “noise” [18].

In this simulation, it is possible that the randomness of certain elements would have a great impact on the results. For example, the target placement algorithm used for this simulation places the target on a purely random matrix. The truth and false assignment of the targets is random and the declaration and attack algorithm is based on a random draw. Hence, the random numbers generated by the computer have a great dominance over how well the search, declaration, and attack would occur. In some cases, the random number generators used for these purposes will tend to produce a bias that would be difficult to detect and remove, thus endangering the validity of such simulation experiments. Random numbers generated by a computer are necessarily deterministic and not truly random since they are produced by algorithms that simulate a randomly generated series. The series repeats itself after some period and the length of this period is a function of the seed used.

In order to eliminate such erroneous results due to statistical uncertainty a Monte Carlo analysis was carried out with a sample size of 100, where the efficiency increases as the dimension of the problem increases.

Comparison of Results

Computer simulation results were obtained for 100 runs for each subject vehicle. The average values for number of true and false encounters, number of target attacks (NTA), number of false target attacks (NFTA), and number of kills (NTK) are listed in Table 4 below.

Table 5 gives the results of the values obtained from analytical calculation of both the parameter in simulation and expected number of true and false attacks obtained from equations (28) and (30). It should be noted that the number of warheads was considered to be a large number (100 for this case), i.e., vehicle has sufficient amount of warheads to attack all targets that it encounters.

Table 4. Simulation Results of the Search and Attack Algorithm for the Subject Vehicles

Output Parameter	Vehicle		
	Nominal Vehicle	Dump Truck	K-8 Jet Trainer
Actual True Target Encounters	4.44	4.54	4.22
Actual False Target Encounters	8.96	9.14	7.86
P_{TR}	0.84	0.995	0.705
Number of "True" Declarations	3.7296	4.5	2.9751
NTA	2.535	2.81	2.395
P_{FTR}	0.95	0.95	0.95
Number of "False" Declarations	0.448	0.457	0.393
NFTA	0.25	0.235	0.26
P_K	0.8	0.8	0.8
NTK	2.01	2.245	1.925

Table 5. Analytical Results of the Search and Attack Algorithm for the Subject Vehicles

Vehicle	Analytical Results of the ATR Algorithm used in the Simulation					Analytical Results from Probability Theory	
	True Encounters	False Encounters	NTA	NFTA	NTK	E(t)	E(f)
Nominal Vehicle	5	10	4.2	0.5	3.36	4.2	0.5
1/20 Tamiya Dump Truck	5	10	4.975	0.5	3.98	4.985	0.5
K-8 Jet Trainer	5	10	3.5	0.5	2.8	3.5	0.5

The values of P_{TR} and P_{FTR} determine the probabilities of true and false declarations, hence, the fraction of the number of true or false attacks respectively. The probability of kill (P_K) will determine the fraction of the attacked targets that will actually be killed. This can be illustrated by applying equations (18) and (19) derived earlier for the case of the dump truck. Then the number of true target attacks,

$$\text{NTA} = \text{True Encounters} \times P_{TR}$$

$$\text{NTA} = 5 \times 0.995 = 4.975.$$

Number of false target attacks,

$$\text{NFTA} = \text{False Encounters} \times (1- P_{FTR})$$

$$\text{NFTA} = 10 \times 0.05 = 0.5.$$

Number of target kills,

$$\text{NTK} = \text{NTA} \times P_K$$

NTK = 3.98.

It is seen from Tables 4 and 5 that the expectant values from analytical calculations show close similarities to the results obtained from the simulation. There are several reasons as to why the analytical and experimental values are different:

1. The vehicle is performing search and attack as it moves forward. Thus it spends some time on attacking that it would have otherwise spent on searching more targets. It also loses coverage over a certain amount of area (due to dead distance) when it switches back from attack to search mode, and when time is expended. Table 6 below shows the average percentage of time the vehicle spends in attack mode and the average percentage of area it fails to cover due to attack. The percentage of area coverage lost due to attack is almost similar to the percentage of targets the vehicle is unable to engage.

Table 6. Average Percentages of Missed Targets, Time Spent in and Area Lost due to Attack mode

Vehicle	Expected number of Encounters	Number of Encounters	Number of Attacks	% Targets detected	% True declarations not engaged	% Area searched
Nominal Vehicle	15	13.4	2.785	89.33 %	33.33 %	93.28 %
1/20 Tamiya Dump Truck	15	13.68	3.045	91.2 %	38.78 %	95.87 %
K-8 Jet Trainer	15	13.32	2.65	80.5 %	21.17 %	87.03 %

2. If the sensor encounters more than one target in the same footprint at a given time, it will decide to attack only the true target that it saw first, and not attack the other true targets that it detected. Hence the number of target attacks will be less than the number of true detections that the vehicle makes.

From the results obtained it is seen that the output parameters show close similarities to each other for the three cases. Thus it can be said that the behavior of the subject vehicles under the ATR algorithm is similar to a great extent. As the vehicle moves faster, the values of each of the output parameters decrease. This is because as the vehicle moves faster, it can generate a larger footprint, and therefore it may be able to detect more targets in a single footprint. Also, as the turn radius increases, the time spent on making maneuvers (during attack) increases, thereby reducing the total area coverage of the battle space.

V. Conclusions and Recommendations

Summary

This research investigated the possibilities and basic methods of scaling flight and sensor dynamics, characteristics, and experimentation of wide area search vehicles. This was accomplished primarily by applying the Buckingham Pi theorem to the governing equations of the system. To allow this, all equations and simulations were defined in non-dimensional terms. The vehicle dynamics and sensor behavior were studied for a basic wide area search vehicle, to identify design variables to develop seven pi groups. Comparisons were made between three vehicles: a nominal vehicle, a slower vehicle and a faster moving vehicle for the purpose of studying the possibilities and effects of scaling.

A MATLAB simulation was developed and the behavior of the vehicle parameters was observed by fixing two parameters. This was done by breaking the simulation to run under two options:

- Fixed velocity and g limit
- Fixed target size and g limit

The simulation was then further developed enabling the vehicle to search a battle space that has a Poisson distribution of true and false targets. The results rendered by the three different vehicles for the search, declaration and attack algorithm were comparatively similar. The numbers were compared with the expected values for true and false attack under probability theory.

Contributions

This research provided a baseline for scaling flight tests of wide area search vehicles and their sensors. The important fact is that the methodology used in this research is not problem specific; and hence, can be used for a wide range of vehicles that have contrasting performance capabilities.

In the experiment developed it was seen that the computer simulations closely approximated analytical values. Furthermore, the ATR algorithm delivered consistent results for the three subject vehicles, which had different vehicle dynamics and sensor characteristics. Therefore it can be concluded that the scaling of different parameters of vehicles and their sensors could be achieved to deliver successful results, by using the methodology discussed in this research.

Recommendations for Future Research

The most basic vehicle dynamics and sensor characteristics were considered for the development of pi groups. Additionally, external forces such as winds, friction, aerodynamic loads were purposely ignored for simplicity. Future research could concentrate on incorporating all the vehicle dynamics, operating conditions, and environments into the dimensional analysis.

The current simulation only employed stationary targets. While moving targets add significant level of complication to the search and attack algorithm, it is indeed an aspect that should be addressed as more research in this area continues to develop. In this research, the wide area search vehicle flew over a rectangular battle space with its heading in the North direction, unless when it was in attack mode. A slightly more complicated battle space, searched by a vehicle that is capable of flying in such a manner that it eventually covers all targets, could be simulated in future investigations.

The vehicle performance parameters, which accurately determine the ROC parameter, were not fully addressed at this time. The declaration and attack algorithm is heavily based the ROC parameter and the ROC curve on which the vehicle flies; therefore it is critical that in future research, the ROC parameter be accurately determined.

Finally, measures could be taken to simulate a completely random environment by detecting the seed and trying to eliminate repetition after multiple replications of the same experiment. A better random number generator could be used in order to deliver more accurate results and statistically safe conclusions.

Appendix A. Variation of Parameters

A.1 Nominal Vehicle

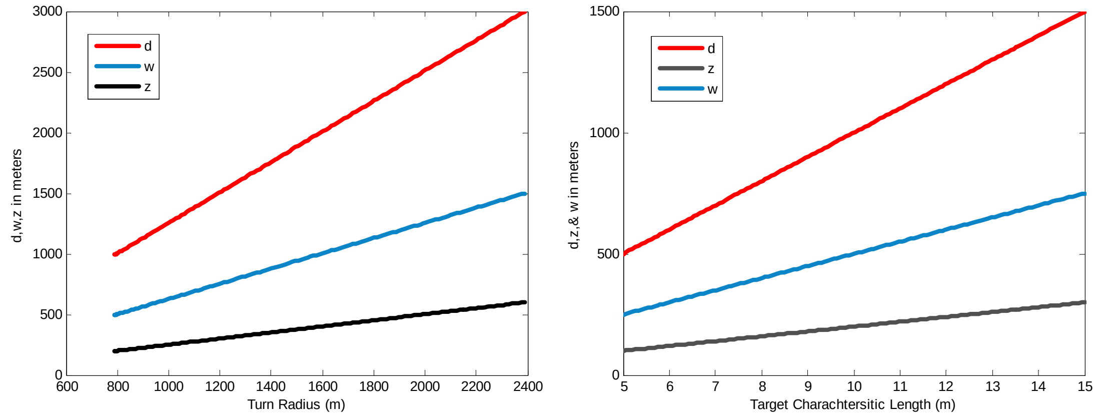

Variation of Dead Range, Footprint Width and Length

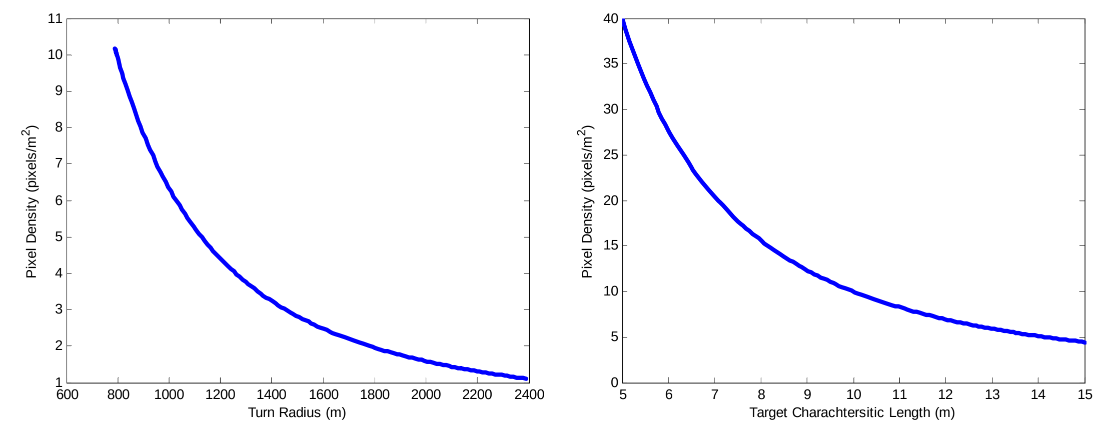

Variation of Pixel Density

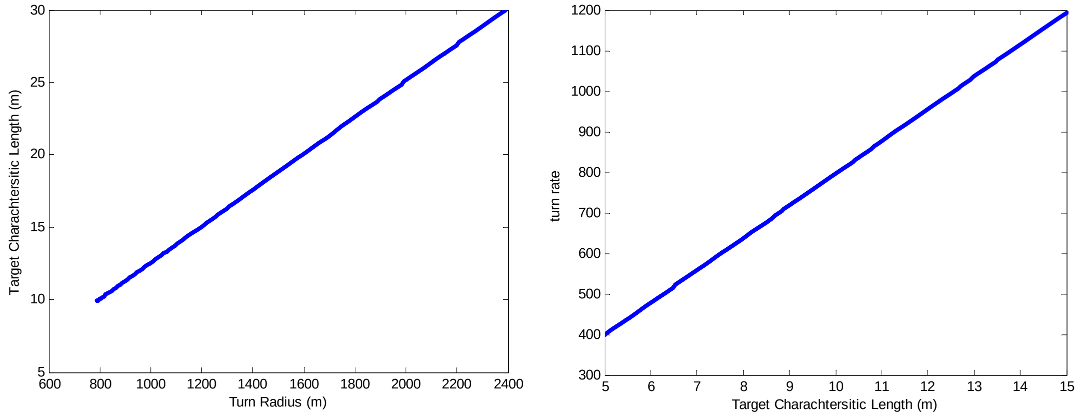

Variation of Target Characteristic Length and Turn Rate

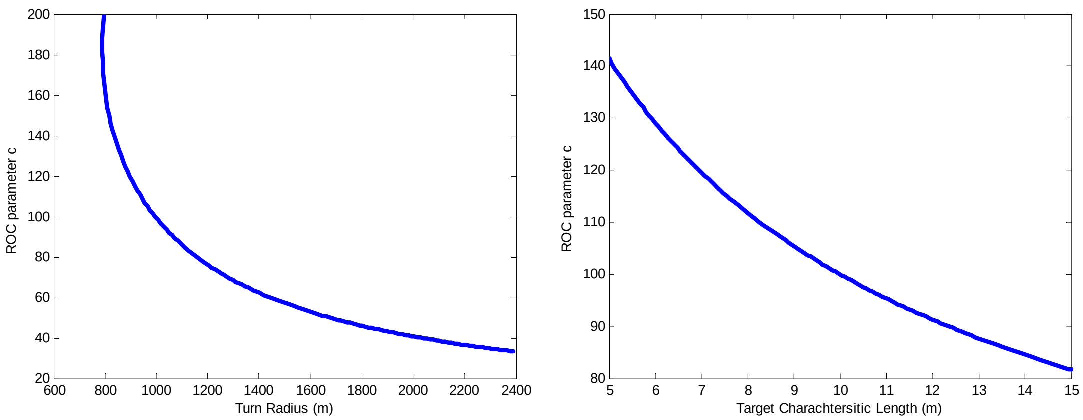

Variation of ROC Parameter

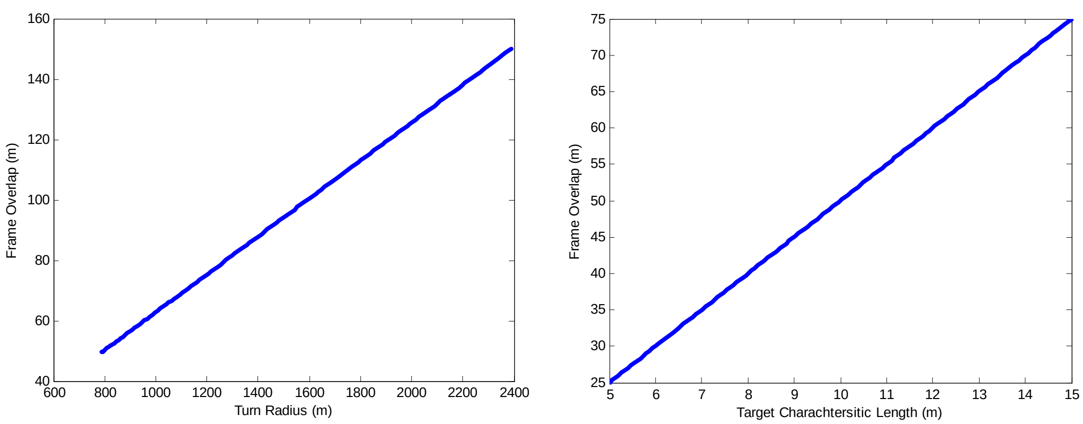

Variation of Frame Overlap

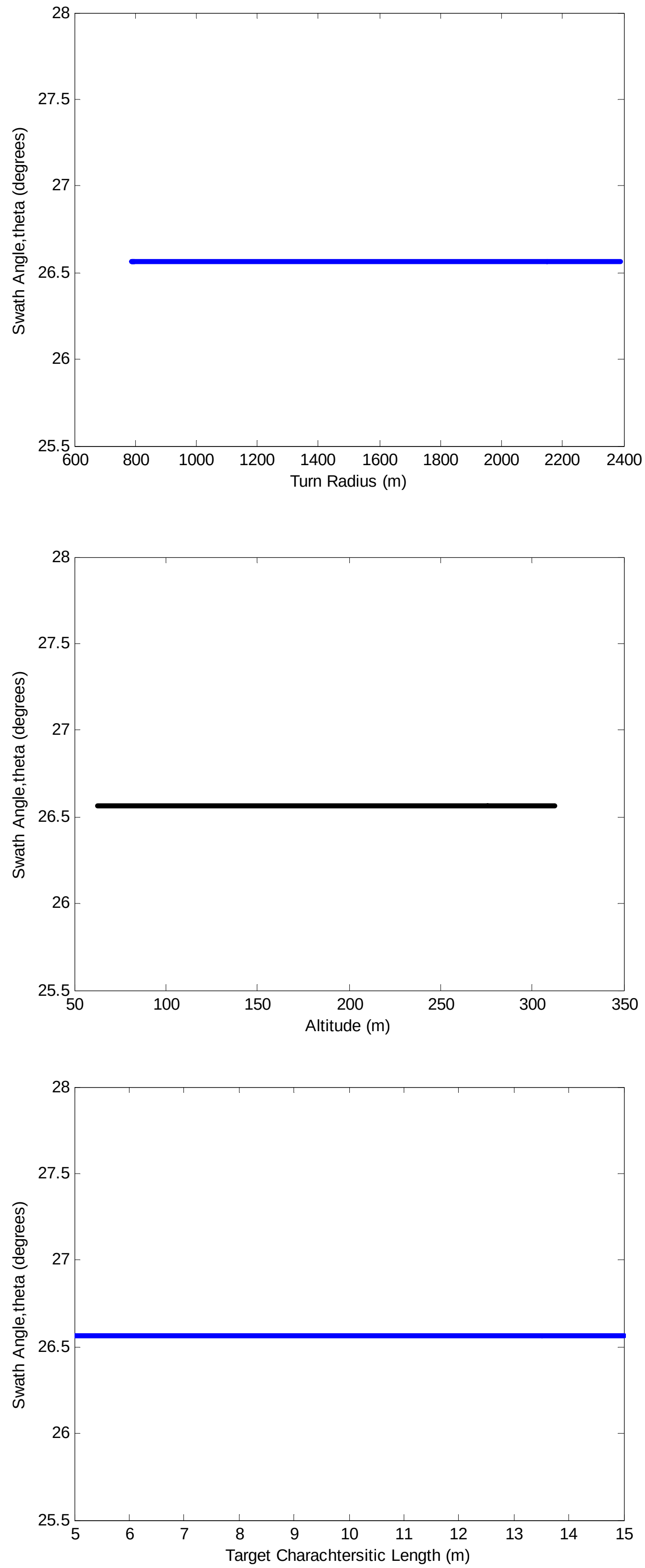

Variation of Swath Angle

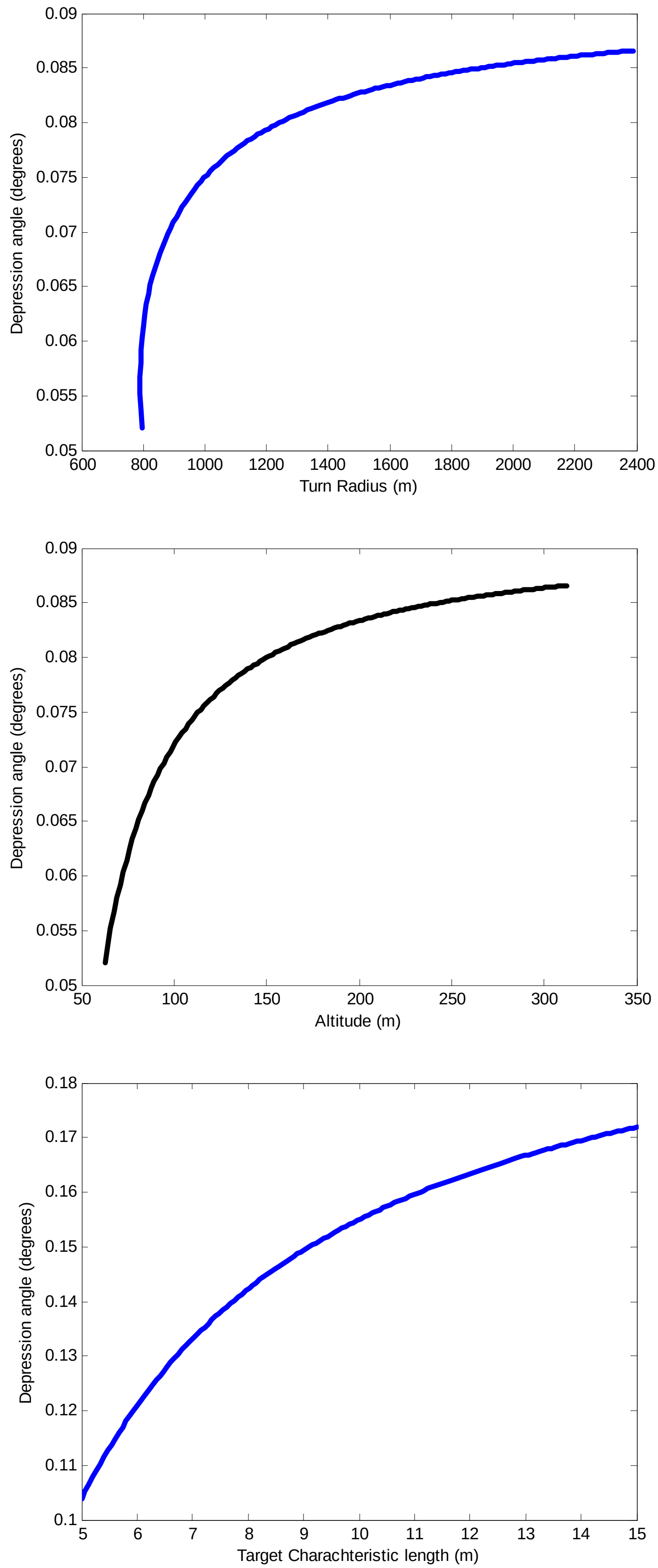

Variation of Depression Angle

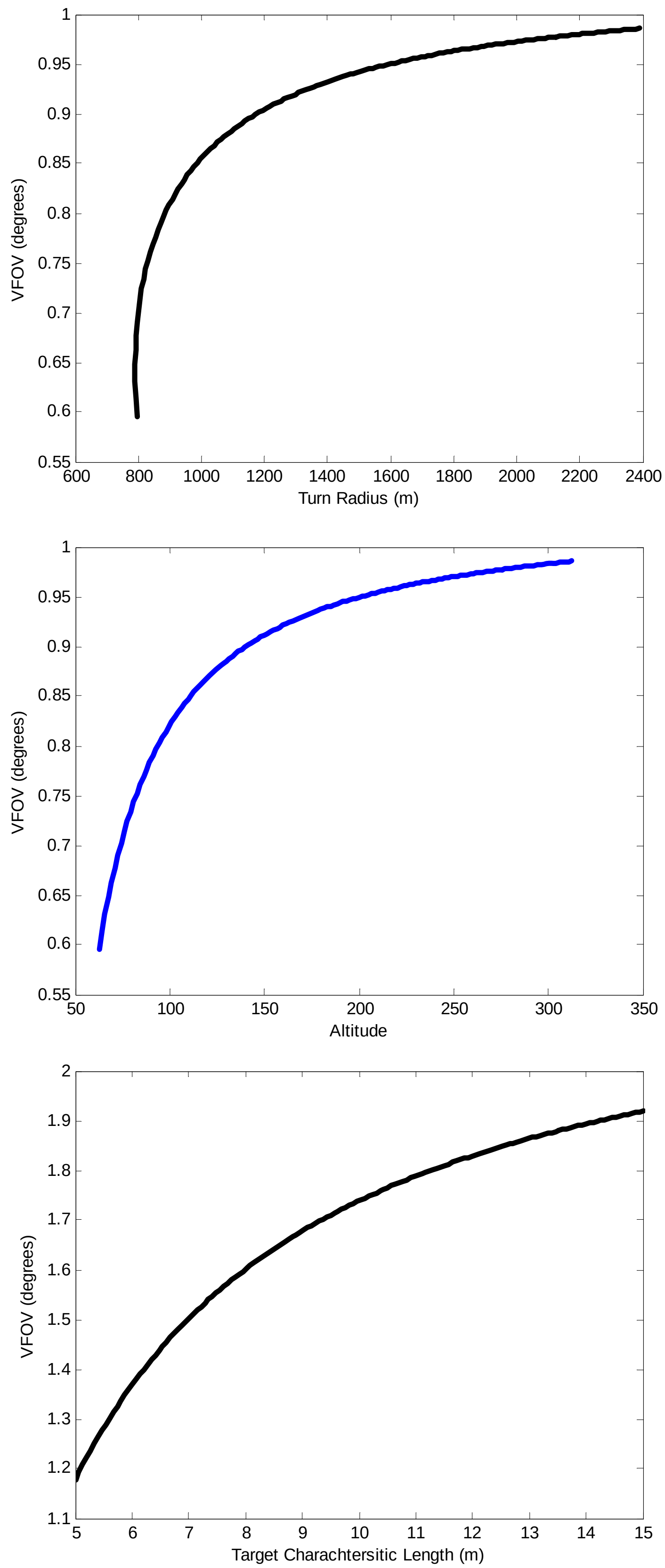

Variation of Vertical Field of View

A.2 Tamiya 1/20 Mammoth Dump Truck

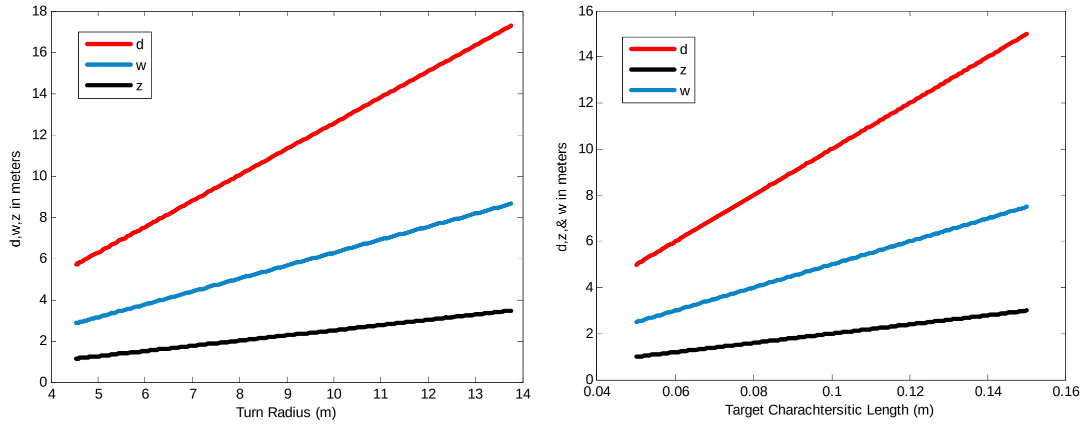

Variation of Dead Range, Footprint Width and Length

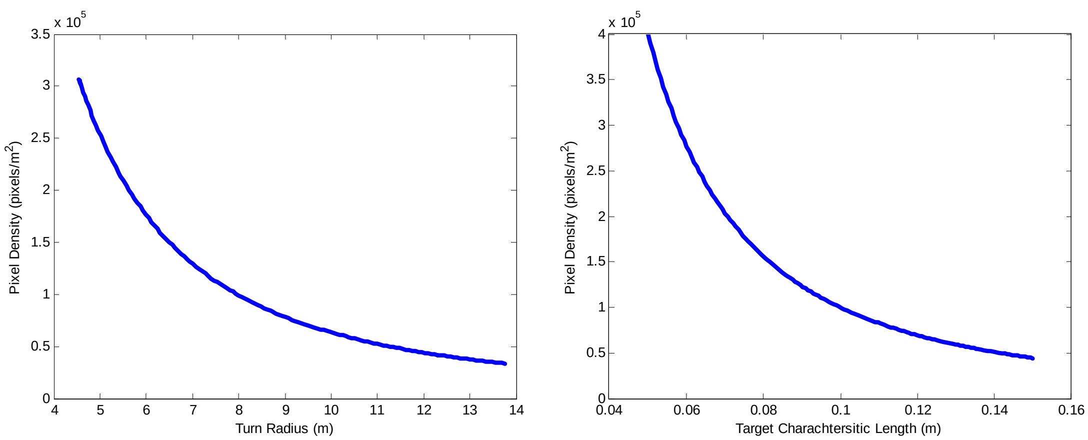

Variation of Pixel Density

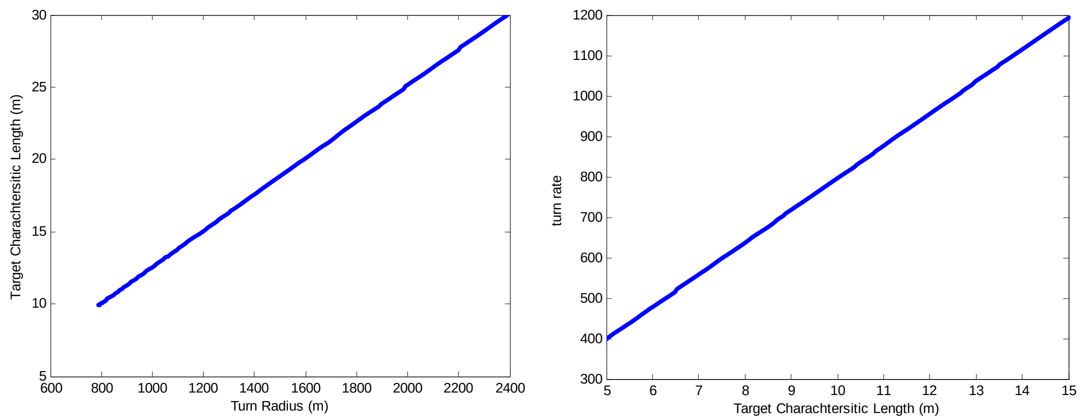

Variation of Target Characteristic Length

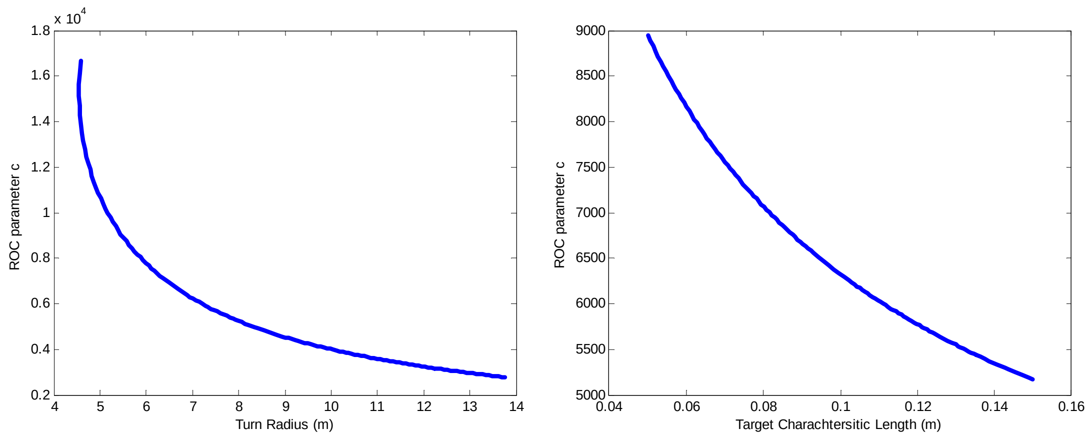

Variation of ROC Parameter

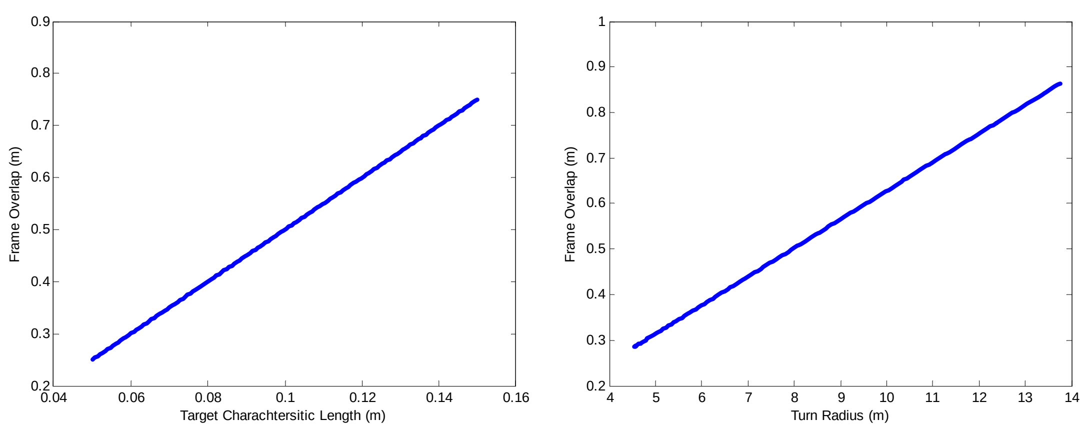

Variation of Frame Overlap

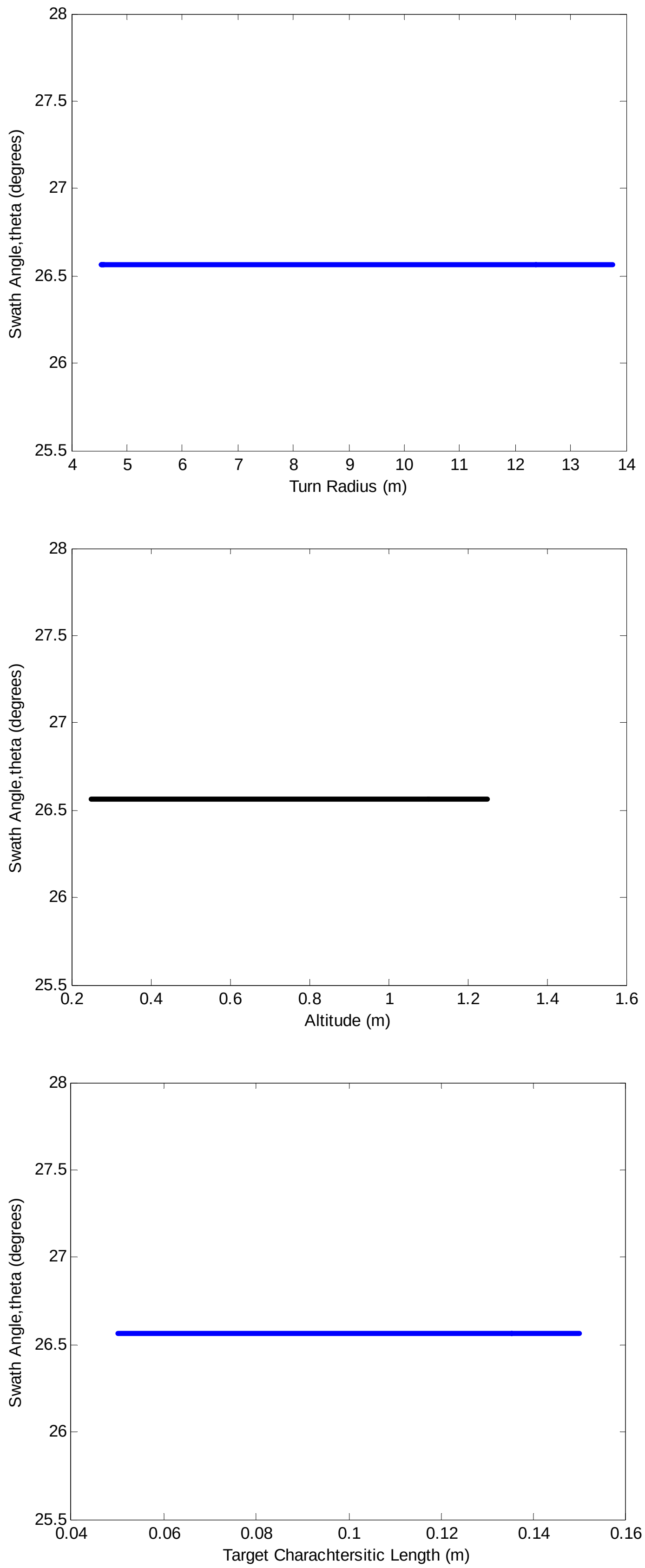

Variation of Swath Angle

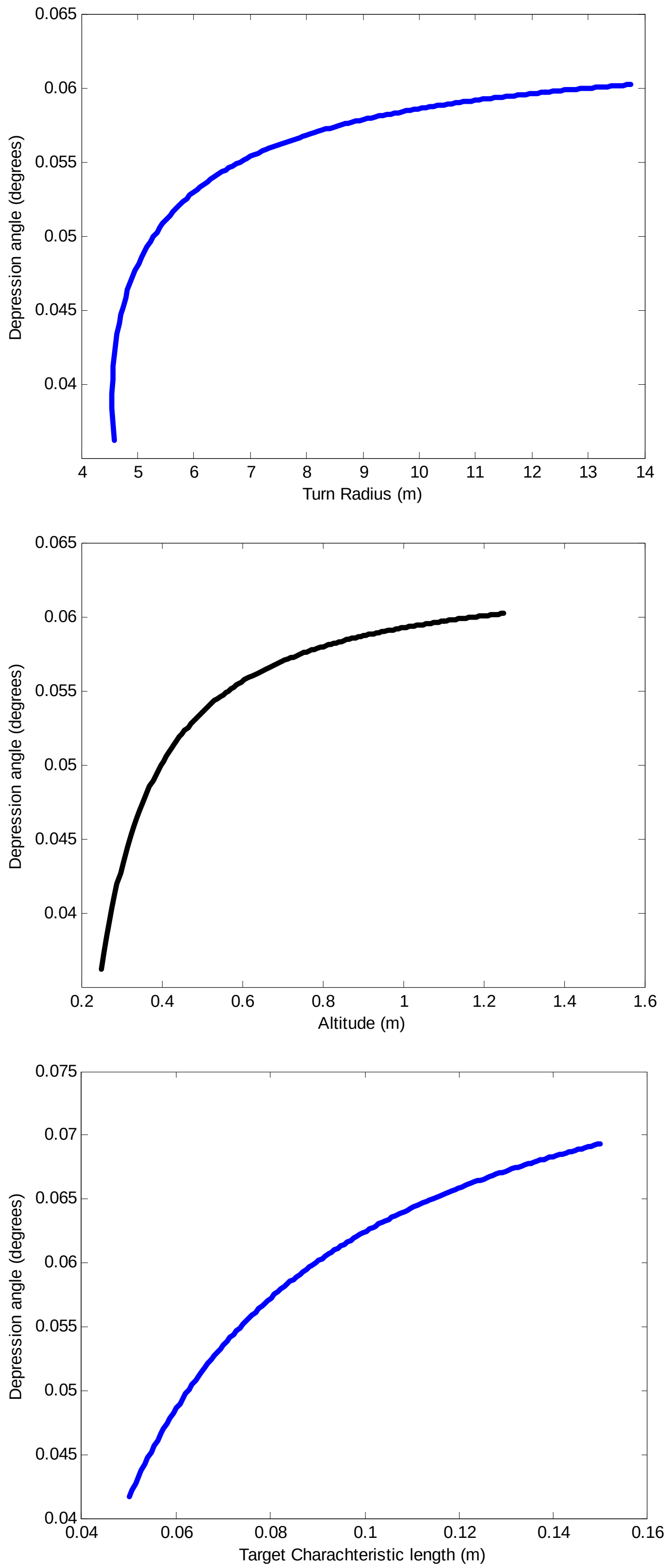

Variation of Depression Angle

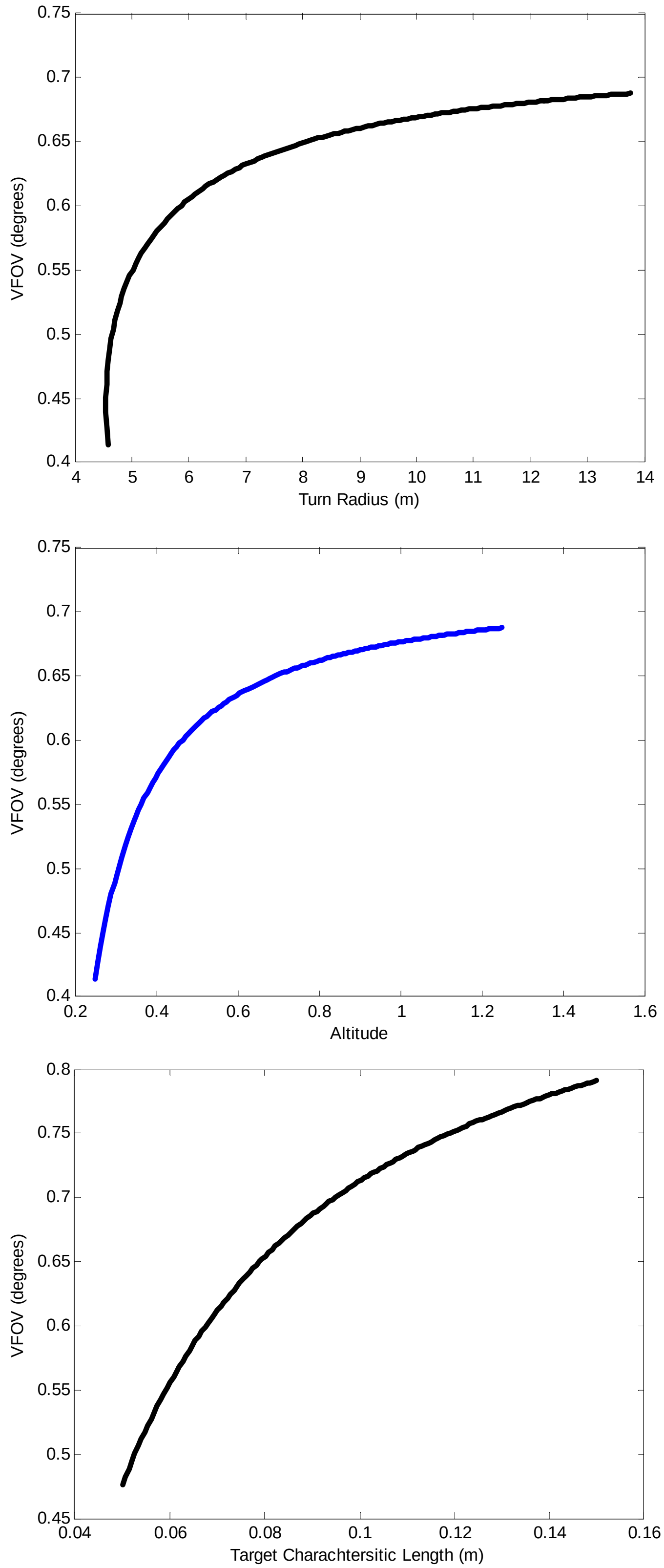

Variation of VFOV

A.3 K-8 Jet Trainer

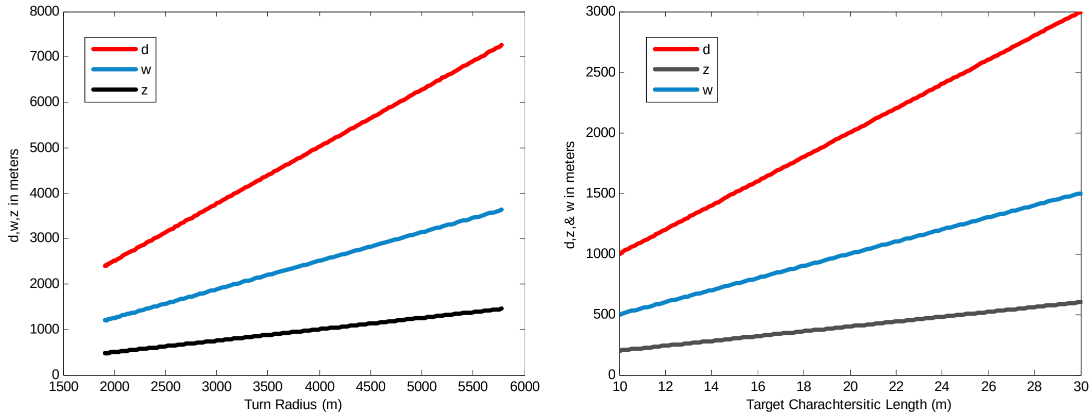

Variation of Dead Range, Footprint Width and Length

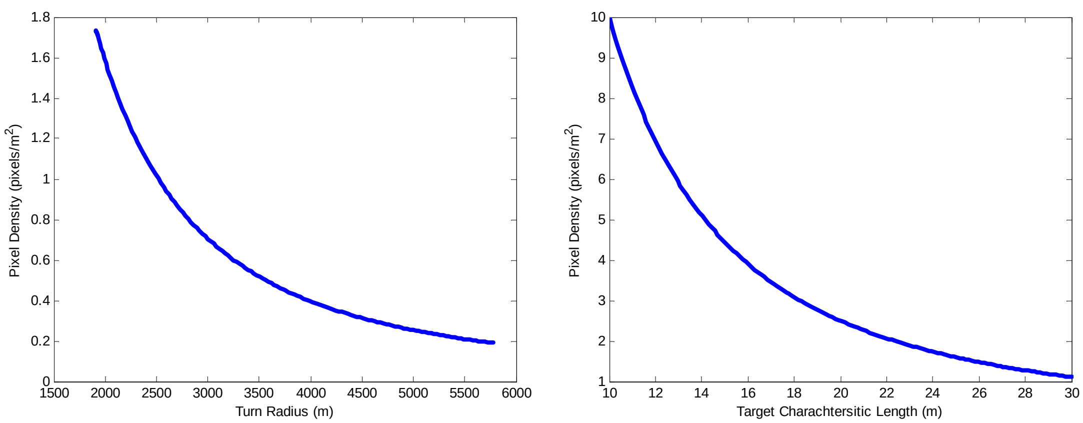

Variation of Pixel Density

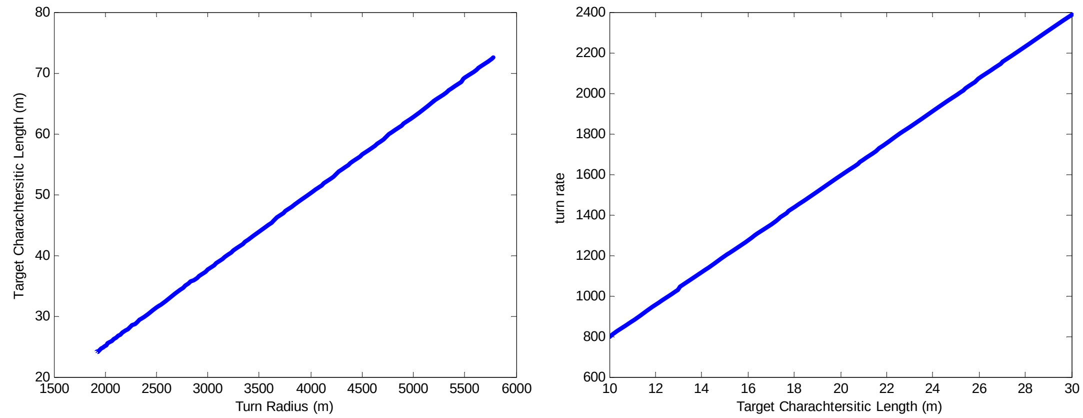

Variation of Target Characteristic Length and Turn Radius

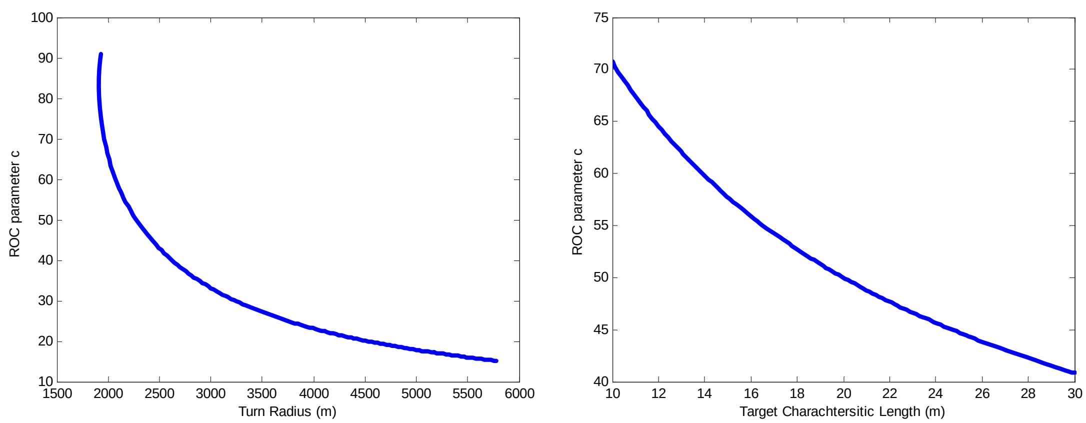

Variation of ROC Parameter

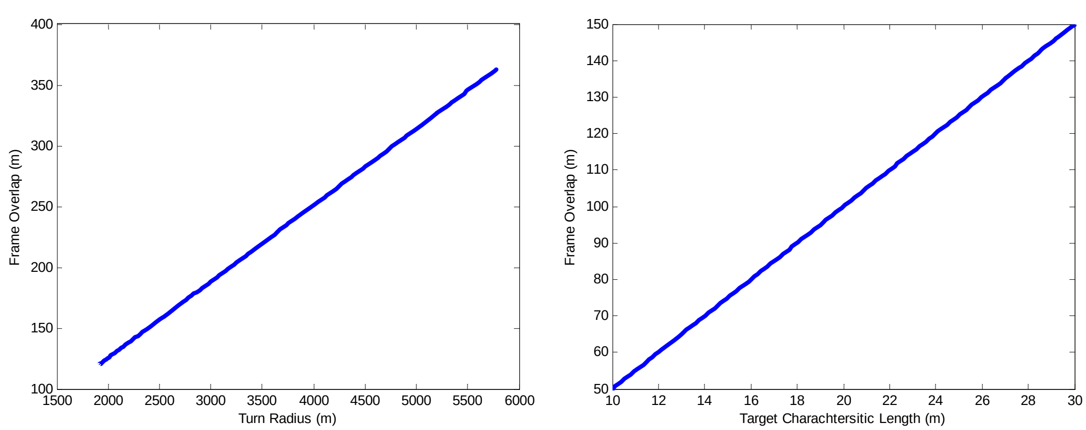

Variation of Frame Overlap

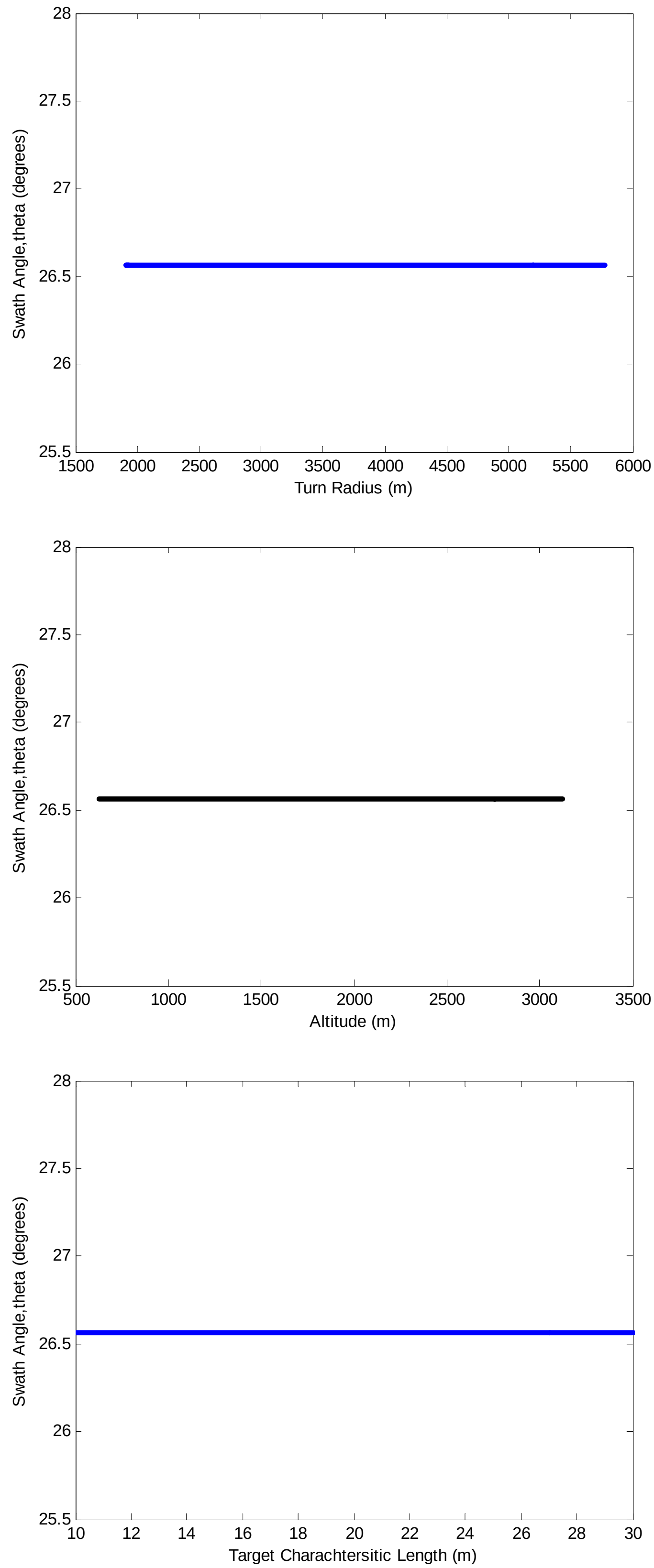

Variation of Swath Angle

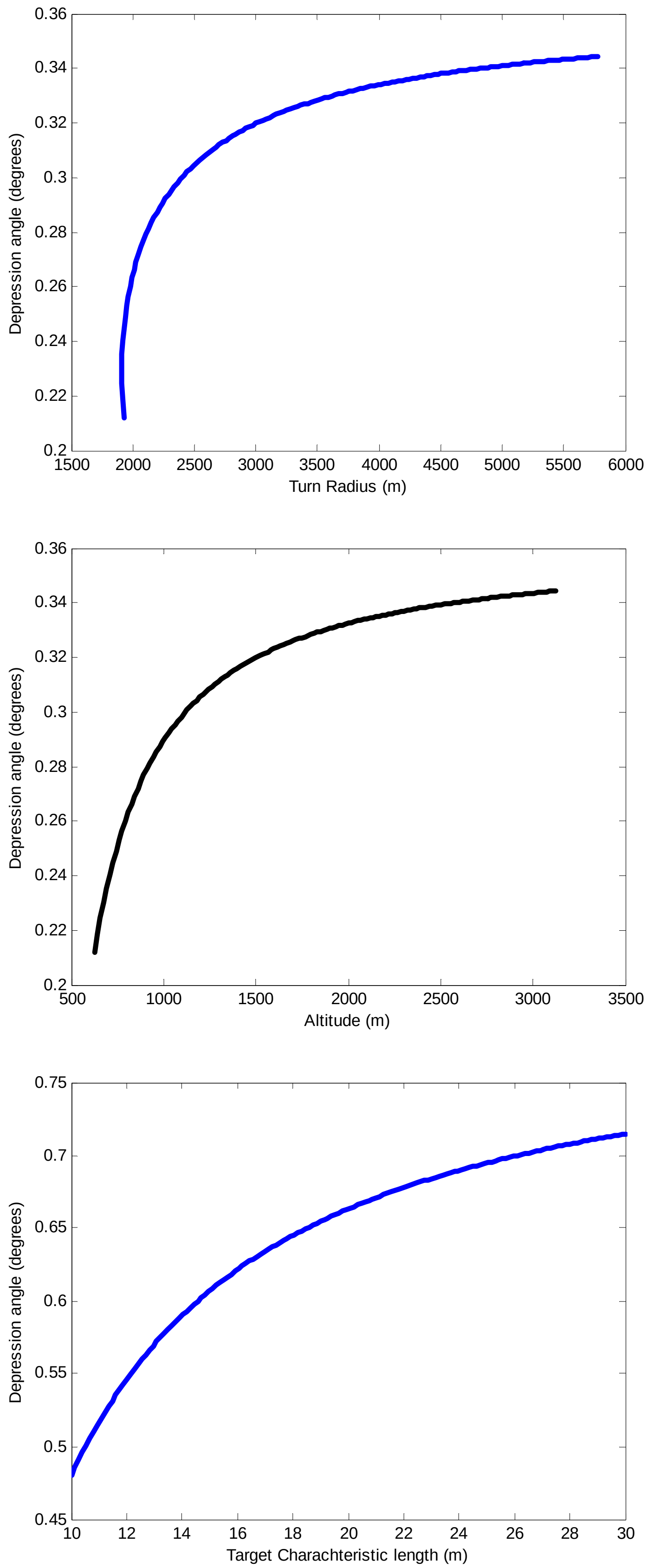

Variation of Depression Angle

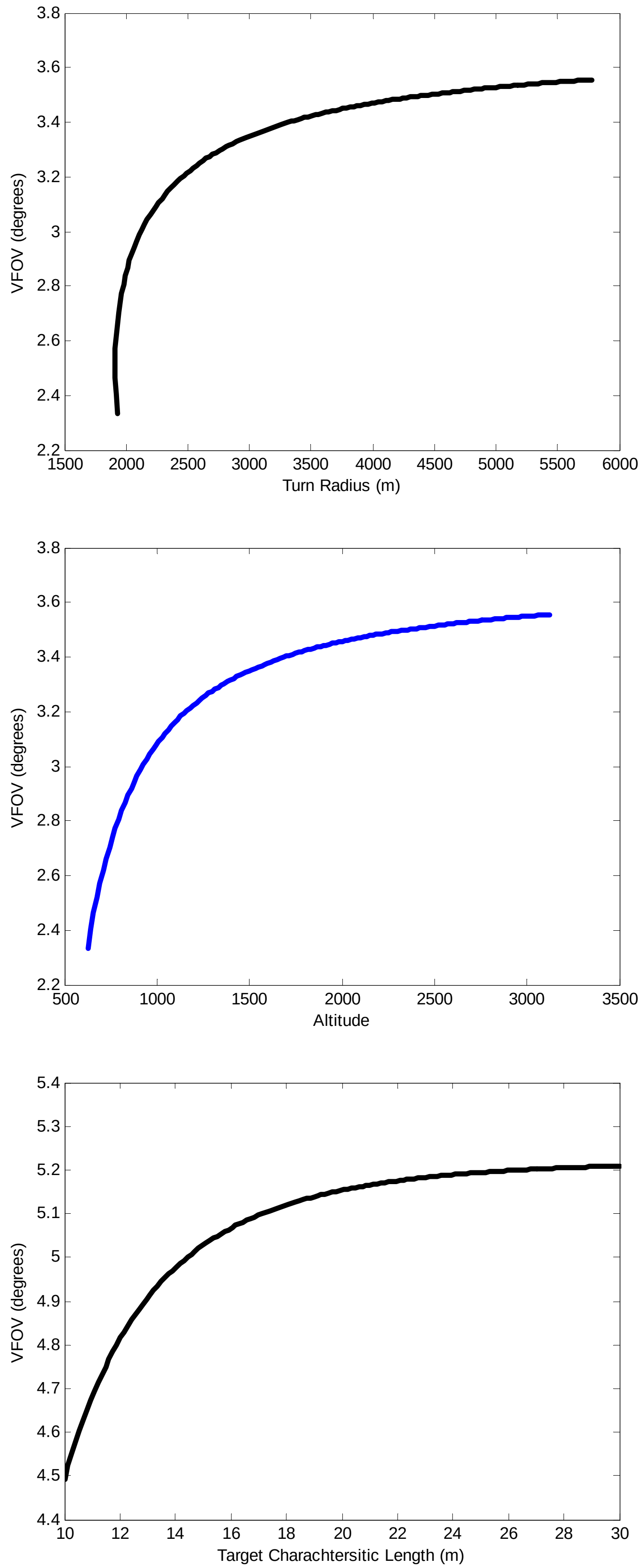

Variation of VFOV

Appendix B. MATLAB Simulation Results

B.1 Basic Results for the Nominal Vehicle

Option 1

The default inputs are:
V_nominal=125 m/sec
g_nominal=2 m/sec^2
d_nominal=1000 m
w_nominal=500 m
z_nominal=200 m
c_nominal=100
pt_nominal=10 1/m^2
P_nominal=10000000 pixels
lt_nominal=10 m
Ol_nominal=50m
Enter 1 to use default values or 0 to enter your own :1
Pi_1:0.2
Pi_2:0.5
Pi_3:1.25568
Pi_4:200000
Pi_5:1e+007
Pi_6:0.01
Pi_7:0.05
Velocity (m/sec):125
turn rate (g"s):2
altitude(m) :250

Velocity,V (m/sec):125
g limit,g (m/sec^2):2
Dead Range,d (m):1000
Footprint length,z (m):200
Footprint width,w (m):500
ROC parameter,c :100
Probability of True Target Report, Ptr :0.840336
Probability of False Target Report, Pftr :0.95
pixels density,rot (1/m^2):10
pixels on target,P_target :100
Target size,lt (m):10
Frame Overlap,Ol (m):50
Azimuthal angle,theta (degrees):26.5544
Elevation angle,alpha (degrees):75.9332
Depression angle,gamma (degrees):11.7683
Vertical Field of View,VFOV (degrees):2.26704

Option 2.

The default inputs are:
V_nominal=125 m/sec
g_nominal=2 m/sec^2
d_nominal=1000 m
w_nominal=500 m
z_nominal=200 m
c_nominal=100
pt_nominal=10 1/m^2
P_nominal=10000000 pixels
lt_nominal=10 m
Ol_nominal=50m
Enter 1 to use default values or 0 to enter your own :1
Pi_1:0.2
Pi_2:0.5
Pi_3:1.25568
Pi_4:1e+006
Pi_5:1e+007
Pi_6:0.01
Pi_7:0.05
Target size:10
g limit:2
altitude(m) :250

Target size,lt (m):10
Dead Range,d (m):1000
Footprint length,z (m):200
Footprint width,w (m):500
Turn Radius,r (m):796.381
ROC parameter,c :100
pixels density,rot (1/m^2):10
pixels on target,P_target :100
Velocity,V (m/sec):125
g limit,g (m/sec^2):2
Frame Overlap,Ol (m):50
Azimuthal angle,theta (degrees):26.5544
Elevation angle,alpha (degrees):75.9332
Depression angle,gamma (degrees):11.7683
Vertical Field of View,VFOV (degrees):2.26704

B.2 Basic Results for the Tamiya 1/20 Mammoth Dump Truck

Option 1.

The default inputs are:
V_nominal=125 m/sec
g_nominal=2 m/sec^2
d_nominal=1000 m
w_nominal=500 m
z_nominal=200 m
c_nominal=100
rot_nominal=10 1/m^2
P_nominal=10000000 pixels
lt_nominal=10 m
Ol_nominal=50m
Enter 1 to use default values or 0 to enter your own :1
Pi_1:0.2
Pi_2:0.5
Pi_3:1.25568
Pi_4:200000
Pi_5:1e+007
Pi_6:0.01
Pi_7:0.05
Velocity (m/sec):1.5
turn rate (g"s):0.05
altitude(m) :1

Velocity,V (m/sec):1.5
g limit,g (m/sec^2):0.05
Dead Range,d (m):5.76
Footprint length,z (m):1.152
Footprint width,w (m):2.88
ROC parameter,c :8333.33
Probability of True Target Report, Ptr :0.997725
Probability of False Target Report, Pftr :0.95
pixels density,rot (1/m^2):301408
pixels on target,P_target :17361.1
Target size,lt (m):0.0576
Frame Overlap,Ol (m):0.288
Azimuthal angle,theta (degrees):26.5651
Depression angle,gamma (degrees):8.2322
Vertical Field of View,VFOV (degrees):1.61681

Option 2.

The default inputs are:
V_nominal=125 m/sec
g_nominal=2 m/sec^2
d_nominal=1000 m
w_nominal=500 m
z_nominal=200 m
c_nominal=100
rot_nominal=10 1/m^2
P_nominal=10000000 pixels
lt_nominal=10 m
Ol_nominal=50m
Enter 1 to use default values or 0 to enter your own :1
Pi_1:0.2
Pi_2:0.5
Pi_3:1.25568
Pi_4:200000
Pi_5:1e+007
Pi_6:0.01
Pi_7:0.05
Target size:0.1
g limit:0.05
altitude(m) :1

Target size,lt (m):0.1
Dead Range,d (m):10
Footprint length,z (m):2
Footprint width,w (m):5
Turn Radius,r (m):7.96381
ROC parameter,c :6324.56
Probability of True Target Report, Ptr :0.997005
Probability of False Target Report, Pftr :0.95
pixels density,rot (1/m^2):100000
pixels on target,P_target :10000
Velocity,V (m/sec):1.97642
g limit,g (m/sec^2):0.05
Frame Overlap,Ol (m):0.5
Azimuthal angle,theta (degrees):26.5651
Depression angle,gamma (degrees):4.76364
Vertical Field of View,VFOV (degrees):0.946951

B.3 Basic Results for the K-8 Jet Trainer

Option 1.

The default inputs are:
V_nominal=125 m/sec
g_nominal=2 m/sec^2
d_nominal=1000 m
w_nominal=500 m
z_nominal=200 m
c_nominal=100
pt_nominal=10 1/m^2
P_nominal=10000000 pixels
lt_nominal=10 m
Ol_nominal=50m
Enter 1 to use default values or 0 to enter your own :1
Pi_1:0.2
Pi_2:0.5
Pi_3:1.25568
Pi_4:200000
Pi_5:1e+007
Pi_6:0.01
Pi_7:0.05
Velocity (m/sec):275
turn rate (g"s):4
altitude(m) :2500

Velocity,V (m/sec):275
g limit,g (m/sec^2):4
Dead Range,d (m):2420
Footprint length,z (m):484
Footprint width,w (m):1210
ROC parameter,c :45.4545
Probability of True Target Report, Ptr :0.705219
Probability of False Target Report, Pftr :0.95
pixels density,rot (1/m^2):1.70753
pixels on target,P_target :41.3223
Target size,lt (m):24.2
Frame Overlap,Ol (m):121
Azimuthal angle,theta (degrees):26.5544
Elevation angle,alpha (degrees):44.0507
Depression angle,gamma (degrees):40.7246
Vertical Field of View,VFOV (degrees):5.20491

Option 2.

The default inputs are:
V_nominal=125 m/sec
g_nominal=2 m/sec^2
d_nominal=1000 m
w_nominal=500 m
z_nominal=200 m
c_nominal=100
pt_nominal=10 1/m^2
P_nominal=10000000 pixels
lt_nominal=10 m
Ol_nominal=50m
Enter 1 to use default values or 0 to enter your own :1
Pi_1:0.2
Pi_2:0.5
Pi_3:1.25568
Pi_4:200000
Pi_5:1e+007
Pi_6:0.01
Pi_7:0.05
Target size:20
g limit:4
altitude(m) :2500

Target size,lt (m):20
Dead Range,d (m):2000
Footprint length,z (m):400
Footprint width,w (m):1000
Turn Radius,r (m):1592.76
ROC parameter,c :50
Probability of True Target Report, Ptr :0.724638
Probability of False Target Report, Pftr :0.95
pixels density,rot (1/m^2):2.5
pixels on target,P_target :50
Velocity,V (m/sec):250
g limit,g (m/sec^2):4
Frame Overlap,Ol (m):100
Azimuthal angle,theta (degrees):26.5544
Elevation angle,alpha (degrees):38.6443
Depression angle,gamma (degrees):46.1691
Vertical Field of View,VFOV (degrees):5.16897

Bibliography

1. G. Galilei, *Disclosure and Mathematic Demonstrations Concerning Two Sciences Pertaining to Mechanics and Local Motions*, 1638.

2. T.A. McMahon and J.T. Bonner*, On Size and Life*. New York: Scientific American, 1983.

3. M.G. Bekker*, Introduction to Terrain-Vehicle Systems*. Ann Arbor, MI Univ, of Michigan Press, 1969.

4. S. Brennan, A. Alleyene, *Using a Scale Testbed: Controller Design and Evaluation.* IEEE Control Systems Magazine,15-26, June 2001.

5. A.H Bond and L. Gasser. *Readings in Distributed Artificial Intelligence*. Morgan Kaufmann Publishers, 1988.

6. T. Blanch, R.C. Arkin. *Behavior Based Formation Control for Multi Robot Teams.* AIAA 2004-6490.

7. D.R. Nelson, T.W. McLain, R.S Christiansen, R.W. Beard, D. Johansen. *Initial Experiments in Cooperative Control of Unmanned Air Vehicles*. AIAA 2004-6533 "Unmanned Unlimited" Technological Conference, Workshop and Exhibit. September 2004, Chicago IL.

8. J. Minor, A.J. Thurling, E. Ohmit *VISTA- A 21st Century UAV test bed.* Web site: www.edwards.af.mil/tps/VISTA. Accessed 30 November 2005.

9. J.B. Barlow, W.H. Rae, A. Pope, *'Low-Speed Wind Tunnel Testing'*, New York: John Wiley & Sons Inc., 1999.

10. W. Travis, R. Whitehead, D. M. Bevly, G.T. Flowes, ' *A study of the effects of various vehicle properties on rollover propensity*", 2004-01-2094.

11. J. Sika, J. Hilgert, Ti. Bertram,. J.P. Pauwelussen, M. Hiller, "*Test Facility for lateral control of a scaled vehicle in an automated highway system*", 2003.

12. Alleyne Research Group-Mechanical and Industrial Engineering, University of Illinois at Urbana-Champaign. www.mrroboto.me.uiuc.edu/ Accessed 04 July 2006.

13. D.R. Jacques, M. Pachter, "*A theoretical foundation for cooperative search, classification, and target attack*", Recent Developments in Cooperative Control and Optimization, 2004.

14. D.D. Decker, "*Decision factors for Cooperative Multiple Warhead UAV Target Classification and Attack with Control Applications*", Air Force Institute of Technology, Wright-Patterson AFB, OH. September 2005.

15. M.R. Spiegel. *Schaum's Outline of Theory and Problems of Probability and Statistics*. McGraw-Hill, Inc., 1992.

16. B.A. Kish, *Establishment of a System Operating Characteristics for Autonomous Wide Area Search Vehicles*. Air Force Institute of Technology, Wright-Patterson AFB, OH. September 2005.

17. E. Buckingham, "*On physically similar systems; illustrations of the use of dimensional equations*," Physical Rev., vol. 4,pp.345-376, 1914.

18. M. Flint, E. Fernandez, W.D. Kelton, "*Simulation Analysis for UAV search algorithms design using approximate dynamic programming*", May 5, 2006.

Vita

Captain Jeevani I. Abeygoonewardene is an officer of the Sri Lanka Air Force. She entered the Sir John Kotelawala Defense Academy, the only tri service academy in South Asia in 1998, and graduated with a Bachelor of Science degree in Aeronautical Engineering in 2002. She was commissioned in the Regular Air Force, and recognized as a Distinguished Graduate.

Her first assignment was at Katunayaka SLAFB as a flight line maintenance officer at No.14 Jet Training squadron. In September 2003 she was assigned to the Aircraft Engineering Wing, which is the main overhaul and heavy maintenance shop of the Sri Lanka Air Force, where she served as the officer in charge of helicopter rotor component overhaul. In August 2004, she entered the Graduate School of Engineering and Management, Air Force Institute of Technology. Upon graduation, she will resume duties as an aircraft maintenance officer in the Sri Lanka Air Force.

REPORT DOCUMENTATION PAGE	*Form Approved* *OMB No. 074-0188*

1. REPORT DATE *(DD-MM-YYYY)*	**2. REPORT TYPE**	**3. DATES COVERED** *(From – To)*
14-Sep-06	**Master's Thesis**	Aug 2004 – Sep 2006

4. TITLE AND SUBTITLE	
Scaling Flight Tests of Unmanned Air Vehicles	**5a. CONTRACT NUMBER**
	5b. GRANT NUMBER
	5c. PROGRAM ELEMENT NUMBER
6. AUTHOR(S)	**5d. PROJECT NUMBER**
Abeygoonewardene, Jeevani, I.,Captain, SLAF	**5e. TASK NUMBER**
	5f. WORK UNIT NUMBER

7. PERFORMING ORGANIZATION NAMES(S) AND ADDRESS(S)	**8. PERFORMING ORGANIZATION REPORT NUMBER**
Air Force Institute of Technology Graduate School of Engineering and Management (AFIT/EN) 2950 Hobson Way WPAFB OH 45433-7765	AFIT/GAE/ENY/06-S01
9. SPONSORING/MONITORING AGENCY NAME(S) AND ADDRESS(ES)	**10. SPONSOR/MONITOR'S ACRONYM(S)**
N/A	**11. SPONSOR/MONITOR'S REPORT NUMBER(S)**

12. DISTRIBUTION/AVAILABILITY STATEMENT

APPROVED FOR PUBLIC RELEASE; DISTRIBUTION UNLIMITED.

13. SUPPLEMENTARY NOTES

14. ABSTRACT

Increasing technological advances and research interest in unmanned air vehicles (UAVs), have led to the need for having safe, inexpensive and effective means of experimenting with their fight performance and surveillance capabilities. Work has previously been done in areas of controlling, analyzing, and predicting cooperative and autonomous operations of UAVs and other vehicles. In addition, there are well established guidelines for scaling experiments in fluid mechanics, where geometric, kinematic and dynamic similarity is obtained by formulating problems in terms of non dimensional variables using dimensional analysis. However, little or no work has been done in developing experiments or guidelines for air vehicles and their sensors. The currently available experiments for such purposes, which are designed around commercially available equipment, have not been standardized and cannot be related to the real systems and the real requirements.

The analysis done in this research provides an important step in setting up guidelines for experimental scaling of flight tests of UAVs. This makes it possible to use computer simulations and ground hardware experiments in a useful way for performance evaluations before having to fly the actual vehicle. Equations and simulations used have been defined in non-dimensional terms in order to allow for a scale independent approach as per the Buckingham Pi theorem. Comparisons have been drawn of flight and sensor performance characteristics between a nominal wide search area vehicle and two surrogate hardware systems having widely varying operating characteristics.

15. SUBJECT TERMS

Autonomous wide area search, experimental scaling, dynamic similarity

16. SECURITY CLASSIFICATION OF:			**17. LIMITATION OF ABSTRACT**	**18. NUMBER OF PAGES**	**19a. NAME OF RESPONSIBLE PERSON**
					Dr. David R. Jacques - ENY
REPORT	**ABSTRACT**	**c. THIS PAGE**			**19b. TELEPHONE NUMBER** *(Include area code)*
U	**U**	**U**	**UU**	106	(937) 255- 3355, ext 3329; e-mail: david.jacques@afit.edu